Stokes number and coupling effects on particle interaction behavior in turbulent channel flows

D. A. Rupp ; L. F. Mortimer ✉ ; M. Fairweather

Check for updates

CrossMark

View
Online

Export
Citation

Stokes number and coupling effects on particle interaction behavior in turbulent channel flows

View Online　　Export Citation　　CrossMark

D. A. Rupp, (ID) L. F. Mortimer,[a] (ID) and M. Fairweather (ID)

AFFILIATIONS

School of Chemical and Process Engineering, University of Leeds, Leeds LS2 9JT, United Kingdom

[a]Author to whom correspondence should be addressed: pmdr@leeds.ac.uk

ABSTRACT

The effects of Reynolds number ($Re_\tau = 180$ and 300), particle Stokes number ($St^+ = 0.5$, 50, and 92), and fluid–solid phase coupling level (one-way, two-way, and four-way) on particle behavior in turbulent channel flows has been investigated using direct numerical simulation and Lagrangian particle tracking. Previous studies have used all these levels of coupling, but in terms of those employing four-way coupling, no consideration is given as to how emergent phenomena due to collision dynamics within a flow affect the way in which particles impart feedback to the continuous phase. In the present work, we relate the particle–particle interaction to particle–fluid coupling, as well as in assessing its relation to the Stokes number. As the Reynolds number increases and the turbulent region narrows, fewer particles retain their velocity as they migrate to the wall-region leading to reduced streamwise velocity fluctuations and preferential concentration. It is also evident that low Stokes number particles are capable of minor wall-accumulation at $Re_\tau = 300$. At this increased Reynolds number, four-way coupled simulations performed with moderate Stokes number particles ($St^+ = 50$) are shown to diminish the effects of particle–fluid feedback, leading to similar fluid and particle statistics as the one-way coupled simulations. It is concluded that turbophoretic and preferential concentration effects are responsible for this phenomenon, since the increased collision rates due to larger concentrations of particles and velocity fluctuations in the wall-region correlate directly with the impact on the two-way coupling flow modifications. Analysis of the collision dynamics also indicates particles colliding with increased relative velocities and angles, which cause larger momentum transfer and directional redistribution, increasing and redirecting slip velocities. It is concluded that for midrange Stokes numbers, four-way coupling is imperative to increase simulation accuracy beyond that obtained assuming one-way coupling.

I. INTRODUCTION

Particle-laden flows are ubiquitous among many natural processes and industrial systems, such as the formation of river beds (Allison *et al.*, 2017), nanoparticulate vascular drug delivery (Tripathi *et al.*, 2021), and nuclear waste transport (Trojanowicz *et al.*, 2018). In such fields, an understanding of both the particle-scale and bulk-scale dynamics is fundamental to the ability to predict long-term eventualities, such as deposition, formation of agglomerates, and blockages. For instance, the nuclear waste processing industry must possess the ability to determine particle–fluid and particle–particle interaction processes that could lead to further complications in waste transport flows in order to guarantee safety and to optimize economic cost (Cunliffe *et al.*, 2021). In such flows, which are often also turbulent due to the presence of high flow rates, knowledge surrounding turbulent dispersion and its effect on particle–particle collisions is paramount in foreseeing processing issues in current designs, as well as in enhancing the effectiveness of future systems.

In recent years, due to advances in computational performance and capabilities, direct numerical simulation and Lagrangian particle tracking have been proven valuable tools for the prediction of particle-laden turbulent flows, capturing many of the bulk-scale phenomena experimentally observed prior to this advent, such as turbophoresis and preferential concentration. With present experimental probing technologies, computational fluid dynamics now surpasses the resolution of the particle-scale interactions current methods can measure, and therefore proves critical to studying such phenomena. In doing so, due to the lack of experimental findings at that resolution, for reliable results, we are therefore restricted to using first-principles techniques with proven high accuracy (such as direct numerical simulation that resolves all turbulence length and time scales down to the Kolmogorov scale) (Elghobashi, 2019).

Over the past decades, significant contributions have been made in the study of particle-laden turbulent flows in the dilute regime. One-way coupled simulations have revealed that particle migration

and local concentration increases occur primarily through two mechanisms: preferential concentration and turbophoresis. Extensive computational studies (Squires and Eaton, 1991; Eaton and Fessler, 1994) have shown that preferential accumulation is most pronounced at $St_\eta \approx O(1)$, with St_η representing the Stokes number based on the Kolmogorov timescale. At this scale, particles tend to aggregate in regions with low velocity magnitude, a phenomenon also observed experimentally (Fessler et al., 1994). Turbophoresis, on the other hand, refers to the tendency of particles to migrate toward areas characterized by low turbulence kinetic energy, the extent of which has also been shown to scale with the particle Stokes number, as demonstrated by Kuerten and Vreman (2005), Marchioli and Soldati (2002), and Marchioli et al. (2008). As particles approach the wall region, they interact with local turbulence structures, exhibiting a diverse range of behaviors based on their material and inertial properties (Mortimer et al., 2019). In recent years, one-way coupled studies are predominantly focused either on more complex geometries (Liu et al., 2023; Wang et al., 2021) or exploring physics underpinning the fundamentals of particle transport and migration (Zahtila et al., 2023).

Extensive investigations have focused on the one-way coupled regime. However, as the volume fraction of particles in a turbulent flow exceeds a certain threshold ($\phi_P > 0.001\%$), it becomes necessary to consider the influence of the particle force feedback on the turbulent fluid phase (Eaton, 2009). Numerous studies in both isotropic turbulence (Boivin et al., 1998; Lee and Hwang, 2022) and wall-bounded channel flows (Pan and Banerjee, 1996) have established that large particles enhance the turbulence, whereas small particles tend to dampen it. Nevertheless, it has been concluded that this effect is less pronounced in systems with low density ratios, even when the particle Stokes numbers in each system are equivalent (Lucci et al., 2011). Furthermore, at larger Stokes numbers, particles possess greater inertia and are less responsive to rapid changes in the flow conditions. They preferentially accumulate in regions of low turbulence intensity, leading to local attenuation or suppression of the turbulence, acting as obstacles that disrupt the local fluid motion and hinder the energy transfer across the different scales of turbulence (Elghobashi, 2019). In the present study, moderately sized particles (relative to the constant bulk length scale, the channel half-height) will be used ($d_P^* = 0.005$), and the Stokes number will be modified by adjusting the density ratio to isolate effects due particle inertia rather than diameter relative to the local turbulence scales.

At further increased volume fractions ($\phi_P > 0.1\%$), the particle motion in liquid–solid and gas–solid suspensions is governed by both hydrodynamic forces and interactions between the particles themselves, as studied and depicted by the phase diagram of Elghobashi (1994). Prediction of this kind of particle-laden flow numerically poses a significant challenge computationally, as it inherently involves large quantities of particles and collision detection. Studies performed in the last few decades have explored the dynamics of collision-driven particle-laden turbulent fluids (Laín et al., 2002; Vreman et al., 2009; and Zhao et al., 2015). In a study undertaken by Ireland et al. (2016), preferential concentration was examined in four-way coupled isotropic turbulence simulations. The results indicated that particles with low Stokes numbers exhibit a tendency to preferentially accumulate in regions characterized by irrotational dissipation, primarily due to vortex ejection mechanisms. It was additionally found that the statistics of relative particle collision velocities exhibited weak sensitivity to the Reynolds number, particularly for particles with a low Stokes number. Dritselis (2016) studied small particles under both two-way and four-way coupling regimes dispersed within a vertical channel flow. It was demonstrated that, once collisions were accounted for, the microparticles could modify the fluid turbulence statistics even at very low volume fractions [$O(10^{-5})$]. In recent years, the development of various methods to simulate such complex systems has been undertaken. The primary difficulty lies in accurately detecting binary collision pairs of particles. To address this, several algorithms have been proposed, including nearest-neighbor lists (Hoomans et al., 1996) and stochastic models (Oesterle and Petitjean, 1993; Sommerfeld, 2001). In the present study, an efficient, accurate domain partition-based deterministic method of identifying collisions (Chen et al., 1999) is used alongside the hard-sphere model to calculate post-collision positions and velocities.

Particle-laden turbulent flow studies at high density ratios and high Stokes numbers are sparse in the present literature but provide valuable insight into the complex dynamics of collisions that modify particle dispersion, clustering, sedimentation, and transport. The present study aims to answer two important questions surrounding these systems. The first addresses the influence of flow Reynolds number on particle dispersion and particle properties as the turbulent region becomes narrower due to increasing the flow rate. Building on previous studies at a lower Reynolds number (Mortimer et al., 2019; Mortimer and Fairweather, 2020; and Mortimer et al., 2020), we first determine how the dynamics are changed when almost doubling the Reynolds number from $Re_\tau = 180$ to $Re_\tau = 300$, focusing on particle Stokes numbers across the range encountered in various industrial environments, ranging from calcite particles (often used as a simulant for nuclear waste material) in water ($St^+ \approx 0.5$) to air ($St^+ \approx 92$). These particular Reynolds numbers were chosen both to match those studied in single-phase investigations, providing a basis for validation, and, as noted, to demonstrate the effect of modifying the flow rate on particle dynamics to elucidate particle–fluid coupling and turbulence interaction effects. The higher Reynolds number flow also possesses properties of value in understanding particle-laden flow dynamics, containing, as it does, not only fully developed turbulent regions, but a wide turbulent boundary layer where particle motion is affected differently in each wall-normal region allowing for a more thorough analysis into collision behavior within each region. The three Stokes numbers employed also encompass particle behavior in the three key regimes: tracer-like, turbophoresis-driven, and high inertia. Once established, we secondly address the variation of coupling level to determine the emergent behavior and elucidate the dynamics of particle–fluid feedback and interparticle collisions in turbulent channel flows.

II. METHODOLOGY

A. Single-phase channel flow simulation

To generate highly accurate predictions of the flow field that encompasses all relevant turbulence length and timescales, the direct numerical simulation (DNS) code, Nek5000 (Fischer et al., 2008) is utilized. In simulating a turbulent channel flow at shear Reynolds numbers of $Re_\tau = u_\tau \delta / \nu_F = 180$, 300, the Eulerian solver employs a high order ($N = 7$) spectral element method (SEM) to model the fluid phase. In this context, u_τ is the shear velocity, δ is the channel half-height, and ν_F is the fluid kinematic viscosity. The selection of this code was based on its efficient parallelization capabilities and extensive

history of validation. Additionally, the open-source nature of the solver makes it suitable for incorporating additional components. The governing equations for the continuous phase dynamics in dimensionless, incompressible form are the continuity and the Navier–Stokes equations, which can be expressed as follows:

$$\nabla \cdot \boldsymbol{u}_F^* = 0, \qquad (1)$$

$$\frac{D\boldsymbol{u}_F^*}{Dt^*} = -\nabla p^* + \frac{1}{Re_B}\nabla^2 \boldsymbol{u}_F^* + \boldsymbol{f}_{PG}^* + \boldsymbol{f}_{2W}^*, \qquad (2)$$

with $\boldsymbol{u}_F^*(\boldsymbol{x}^*, t^*)$ the fluid velocity vector at position $\boldsymbol{x}^*$ and time, t^*, $p^*(\boldsymbol{x}^*, t^*)$ the fluid pressure, Re_B the bulk Reynolds number defined as $Re_B = U_B\delta/\nu_F$, and $\boldsymbol{f}_{PG}^*$ the constant pressure gradient forcing term. The equations presented above are nondimensionalized utilizing the channel half-height, δ, the bulk velocity, U_B, and the density of the fluid phase, ρ_F. Henceforth, any parameter or quantity marked with an asterisk ($*$) signifies a non-dimensionalized variable obtained using these bulk properties (δ, U_B, ρ_F). To account for the complete two-way momentum exchange between particles within a designated cell and the surrounding fluid, an additional term $\boldsymbol{f}_{2W}^*$ is incorporated. Further information regarding this term will be provided in Sec. II B.

The conservation equations are numerically solved on a discretized, structured Cartesian grid, which consists of $27 \times 18 \times 23$ seventh-order spectral elements, equivalent to approximately 3.9 M nodes. In the wall-normal direction of the channel, the grid is scaled such that the elements closer to the wall are thinner and more densely distributed. The distribution of elements is uniform in the streamwise and spanwise directions. The computational domain (x, y, z) has dimensions $12\delta \times 2\delta \times 6\delta$, representing a channel, with boundary lengths chosen to ensure capture of all the largest vortical structures. The domain is illustrated in Fig. 1.

Here, x corresponds to the streamwise direction, y corresponds to the wall-normal direction, and z corresponds to the spanwise direction. Periodic boundary conditions are imposed at both ends of the streamwise and spanwise axes to ensure the flow remains cyclic. On the wall-normal axis, no-slip and impermeability conditions are enforced at $y^* = \pm 1$. The flow is driven and sustained by a constant pressure gradient applied in the streamwise (x) direction. The magnitude of the pressure gradient prescribed is as follows:

$$\frac{\partial p^*}{\partial x^*} = \left(\frac{Re_\tau}{Re_B}\right)^2. \qquad (3)$$
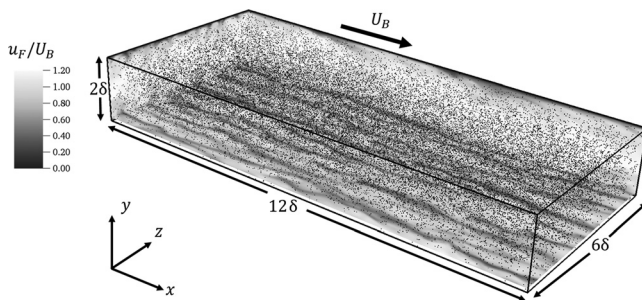

FIG. 1. Schematic of the multiphase turbulent channel flow at $Re_\tau = 180$. Scale indicates fluid velocity magnitude non-dimensionalised by the bulk flow velocity, U_B. Black spheres indicate locations of particles.

As mentioned previously, $Re_\tau = u_\tau\delta/\nu_F$ represents the shear Reynolds number, with $u_\tau = \sqrt{\tau_W/\rho_F}$ the shear velocity and τ_W the mean shear stress at the wall. In Table I, the continuous phase parameters for the single-phase predictions of turbulent channel flow at $Re_\tau = 180$ and 300 are presented. The solver adopts a constant time step of $\Delta t^* = 0.005$ and is initialized with a laminar profile that includes minor perturbations in the off-stream directions to facilitate the transition to turbulence. Convergence to a statistically stationary state is assessed by monitoring the first- and second-order flow statistics. Once convergence is confirmed, further statistics are gathered for validation and analysis purpose.

B. Lagrangian particle tracking

In order to track the trajectories of solid particles through the flow, a Lagrangian particle tracking (LPT) routine was developed, which operates concurrently with Nek5000. Each individual particle in the ensemble is represented as a point-like, impenetrable, and undeformable computational sphere. After completing a time step for the continuous phase, the LPT routine solves the non-dimensional equations of motion for each particle in the system. These equations are derived by considering the force balance between the particle's inertia and the fluid, as described by Maxey (1987) and Riley and Patterson (1974). Consequently, forces other than drag, such as lift, virtual mass, and pressure gradient, are likely to be relevant, as observed in previous studies (Homann and Bec, 2010; Mortimer et al., 2019). Therefore, we consider the contributions from all hydrodynamic forces. Mortimer et al. (2019) provide information on the relevance of these forces based on the distance from the channel wall. The Basset history force is neglected due to the long computation times it entails and previous evidence demonstrating minimal impact on particle motion (Fairweather and Hurn, 2008; Daitche, 2015). Additionally, gravitational and buoyancy forces are disregarded because the focus of this work is on understanding the effects of turbulence on particle dispersion, particle–fluid coupling, and particle–particle interactions, which are still not fully studied or understood, making it challenging to isolate purely turbulence-based effects when these forces are included. For instance, for a horizontal channel flow, including these forces would lead to particle accumulation in the lower half of the channel, reducing the time available to sample particle statistics in the upper half of the domain. It would also lead to additional gravitational contributions to the wall-normal component of the slip velocity, not attributable to the effects of turbulence, which adds additional complexities in analyzing the effect of particle–fluid coupling. For vertical channel flows, the first point is resolved, but there then exists further streamwise slip velocity contributions due to gravitational acceleration, again not attributable to the effects of the fluid conveying motion. We, therefore, choose to

TABLE I. Parameters for DNS of turbulent channel flow. $L_{x,y,z}$ represents the Cartesian lengths of the domain, $E_{x,y,z}$ is the number of elements in each direction, and y_{MIN}^+ is the minimum wall-normal spacing in wall units.

Re_τ	Re_B	$L_x \times L_y \times L_z$	$E_x \times E_y \times E_z$	Δt^*	y_{MIN}^+
180	2800	$12\delta \times 2\delta \times 6\delta$	$27 \times 18 \times 23$	0.005	0.183
300	4900	$12\delta \times 2\delta \times 6\delta$	$27 \times 18 \times 23$	0.005	0.306

restrict the calculations solely to forces exerted due to the fluid. The equations of motion solved for each particle are as follows:

$$\frac{\partial \boldsymbol{x}_P^*}{\partial t^*} = \boldsymbol{u}_P^*, \tag{4}$$

$$\frac{\partial \boldsymbol{u}_P^*}{\partial t^*} = \frac{1}{M_{VM}} \left[\underbrace{\frac{3C_D |\boldsymbol{u}_s^*|}{4 d_P^* \rho_P^*} \boldsymbol{u}_s^*}_{Drag} + \underbrace{\frac{3C_L}{4 \rho_P^*} (\boldsymbol{u}_s^* \times \boldsymbol{\omega}_F^*)}_{Lift} + \underbrace{\frac{1}{2\rho_P^*} \frac{D\boldsymbol{u}_F^*}{Dt^*}}_{Virtual\ Mass} + \underbrace{\frac{1}{\rho_P^*} \frac{D\boldsymbol{u}_F^*}{Dt^*}}_{Pressure\ Gradient} \right]. \tag{5}$$

In Eqs. (4) and (5), $\boldsymbol{x}_P^*$ represents the particle position vector, $\boldsymbol{u}_P^*$ the particle velocity vector, $\boldsymbol{u}_F^*$ the fluid velocity vector spectrally interpolated at the position of the particle, $\boldsymbol{u}_S^* = \boldsymbol{u}_F^* - \boldsymbol{u}_P^*$ the slip velocity between the fluid and the particle, d_P^* the particle diameter non-dimensionalized by the channel half-height, ρ_P^* the density ratio between the fluid and the particle, and $\boldsymbol{\omega}_F^*$ the vorticity of the fluid spectrally interpolated at the particle position, given by $\boldsymbol{\omega}_F^* = \nabla \times \boldsymbol{u}_F^*$. M_{VM} is an added mass modification term given by $M_{VM} = \left(1 + \frac{1}{2\rho_P^*}\right)$. The drag coefficient, C_D, is calculated using the correlations of Schiller and Naumann (1933), where $C_D = 24 f_D / Re_P$, with $f_D = \left(1 + 0.15 Re_P^{0.687}\right)$ when $Re_P > 0.5$ and $f_D = 24 / Re_P$ otherwise (in the Stokes regime). Here, Re_P is the particle Reynolds number, given by $Re_P = Re_B d_P^* |\boldsymbol{u}_S^*|$. Additional information regarding the calculation and origins of these terms can be found in Mortimer *et al.* (2019).

Particle motion is calculated after the completion of a fluid time step. First, using spectral interpolation, the fluid velocity and derivative fields are obtained. Equations (4) and (5) are then integrated using a fourth-order accurate Runge–Kutta scheme, with a time step (Δt^*) equal to that of the continuous phase solver. This integration scheme allows us to determine each particle's new position and velocity. Once the calculations are completed for all particles in the channel, the collision detection and agglomeration determination/resolution algorithm is executed, as explained in detail below. Interactions between particles and the channel walls are detected and resolved using elastic collisions, where the particle's wall-normal velocity is reflected upon colliding with the channel wall. In the periodic directions (streamwise and spanwise), particles that leave the boundary are reinjected at the corresponding location on the opposite side of the computational domain, maintaining the periodic nature of the channel flow.

For higher volume fractions, accurate modeling of the hydrodynamic forces exerted by the dispersed phase on the carrier fluid is essential. To account for each particle's inertial effect on the fluid phase, an additional source term is included in the Navier–Stokes equations. This approach, commonly referred to as the particle-source-in-cell method (Zhao *et al.*, 2015), ensures predictive accuracy. The acceleration term in the Navier–Stokes equations applied to cell i is given by

$$\boldsymbol{f}_{2W}^{*i} = \frac{1}{V_i^*} \sum_{j}^{N_{P,i}} \frac{\partial \boldsymbol{u}_{P_j}^*}{\partial t^*}, \tag{6}$$

where V_i^* is the volume of the computational cell, and j is an index that iterates over the number of particles contained within the corresponding cell, $N_{P,i}$. The LPT routine also incorporates deterministic particle–particle interactions, known as four-way coupling, to accurately simulate systems with higher solid-phase volume fractions. In this case, we employ the hard-sphere elastic collision model, as described in Mortimer *et al.* (2020), which assumes that the contact time during particle collisions is significantly shorter than the LPT integration time step. This assumption holds when the particles are rigid and undeformable. Additionally, the model assumes negligible transfer of rotational momentum during collisions and considers all collisions to be frictionless. We also assume that any other interparticle forces acting over the course of the collision are negligible and that all collisions are binary such that tertiary or larger collision events are sufficiently rare that the resolution of such would improve the accuracy only minimally. Computation times are improved by implementing a deterministic binary collision search algorithm, based on the work of Breuer and Almohammed (2015).

During each time step, the particles are distributed into cells within a secondary coarse mesh, where the number of cells is specified by the user. This process is depicted in the left-hand diagram of Fig. 2. The collision algorithm is then applied to each individual cell in this new mesh, treating each cell as a separate full collision detection domain. The code determines particle collisions by comparing their relative inter-surface displacements and velocities. If both quantities are negative, indicating overlap, then the particles are considered to have collided. This algorithm is applied on all cells, enabling efficient collision detection and reducing the computational complexity from $O(N_P^2)$ to $O(N_P)$, where N_P represents the total number of particles dispersed in the domain. The search for collisions is then repeated on a slightly coarser grid, as shown in the right-hand diagram of Fig. 2. This step helps identify pairs of particles that might have been missed
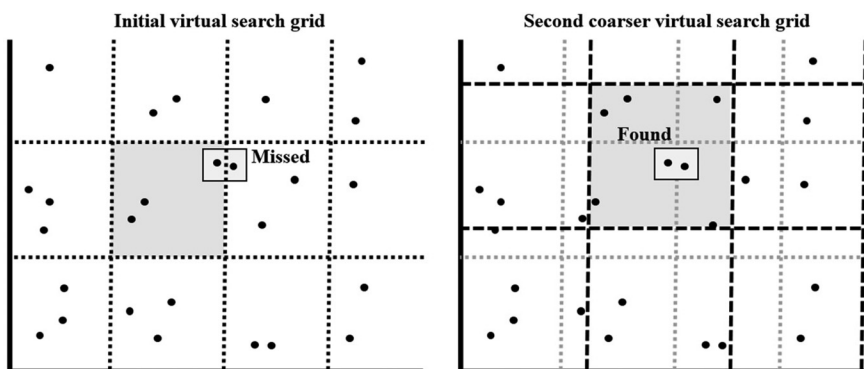
FIG. 2. Initial (left) and secondary (right) search grids for deterministic binary collision identification.

in the initial search. In the present work, we selected a value of 32^3 cells for the initial search and 30^3 cells for the secondary search. This choice balances computational efficiency while ensuring that the initial boxes are sufficiently large to capture most collisions. It is crucial to emphasize that without an algorithm like this, accurately identifying collisions for large numbers of particles would be extremely challenging given current computational resources. To accommodate collisions, the pre-collision velocities and the locations of the two particles are recorded, and standard hard-sphere kinetic energy and momentum conservation principles are employed, following similar approaches in previous works (Mortimer *et al.*, 2020; Yamamoto *et al.*, 2001; and Chen *et al.*, 1999), to determine the resulting velocities of the colliding particles. The simulation parameters for the particulate phase used in this study are presented in Tables II and III.

III. RESULTS AND DISCUSSION

A. Continuous phase validation

Initially, unladen turbulent flow simulations at SEM order $N = 7$ were performed in both channels using different pressure gradient

TABLE II. Fixed particle phase parameters.

Fixed parameter	Value
Number of particles, N_P	300 000
Particle diameter, d_P^*	0.005
Particle volume, V_P^*	6.545×10^{-8}
Volume fraction, ϕ_P	1.4×10^{-4}

TABLE III. Varied particle phase parameters and simulation matrix (1 W signifies one-way coupling, etc.).

			Re_τ					
Variable parameters			180			300		
St^+ 0.5	ρ_P^*	2.5, 4	1 W	—	—	1W	2W	4W
50	(180, 300)	1111, 400	1 W	—	—	1W	2W	4W
92		2041, 736	1 W	—	—	1W	2W	4W

driving force terms in order to establish statistically stationary turbulence fields for $Re_\tau = 180$ and $Re_\tau = 300$. The initial condition for each was identical, using a mean velocity profile with minor perturbations encouraging the transition to turbulence. These were performed for $T_S^* = 100$ non-dimensional time units, with statistics sampled across the final $50 \leq t^* \leq 100$. Statistics were also measured in time intervals across $t^* = 10$ in order to guarantee that there were no variations in the results with time. Figures 3 and 4 illustrate the mean streamwise continuous phase velocity as well as the root mean square (RMS) of the velocity fluctuations and major shear stress. These are compared against the DNS findings of Moser *et al.* (1999) for the $Re_\tau = 180$ simulation and of Marchioli and Soldati (2007) for the $Re_\tau = 300$ simulation. In both cases, the agreement is very good, with only slight deviations in the shear stress profile for the $Re_\tau = 300$ case, which may be due to the fact that in the present case almost twice as many equivalent grid points were used, since the shape of the profile is qualitatively similar to that of the well-validated $Re_\tau = 180$ case. Overall, the validation exhibits excellent agreement and demonstrates confidence in the statistically stationary single-phase in which particles are to be injected.

B. One-way coupled particle statistics

The particle tracking algorithm has been validated against previous studies in our earlier work (Mortimer and Fairweather, 2020); therefore, we begin with consideration of one-way coupled simulations in particle-laden turbulent channel flows, with a focus on the influence of Stokes number and Reynolds number. Initially, the dispersive and particle tendency to preferentially concentrate is studied by restricting the coupling regime to one-way coupling. In this case, the effect of the particles on the surrounding fluid is ignored, as are interparticle collisions. In both channel flows, three particle species were injected possessing Stokes numbers based on the viscous timescale, $St^+ = 0.5$, 50, and 92. These were obtained by varying the particle–fluid density ratio, while keeping the particle diameter constant, in order to preserve the volume fraction in each case, and chosen to represent calcite particles in various media of relevance to industrial flows of decreasing density, from water through air. Particles are injected randomly throughout the domain and are mono-dispersed for each case, ensuring no overlap (though in the one-way coupled simulations, particle–particle
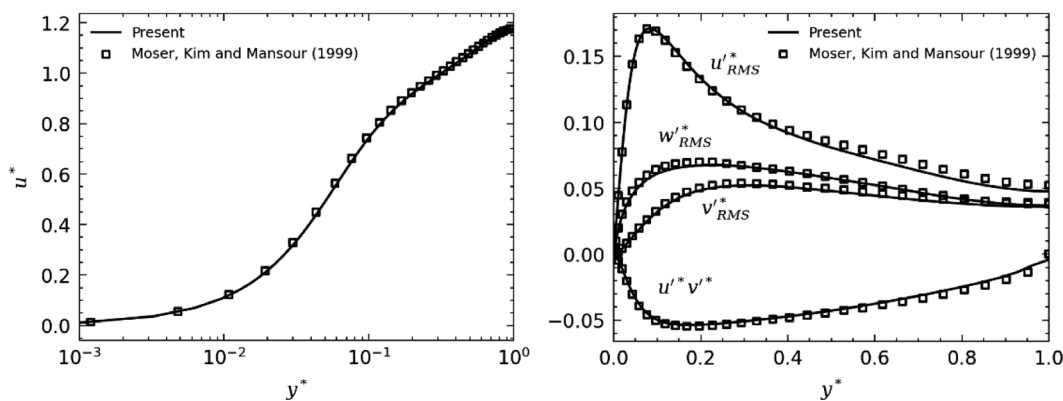

FIG. 3. Profiles of mean fluid streamwise velocity (left) and RMS of velocity fluctuations/shear stress (right) for turbulent channel flow at $Re_\tau = 180$. Findings are compared to Moser *et al.* (1999).
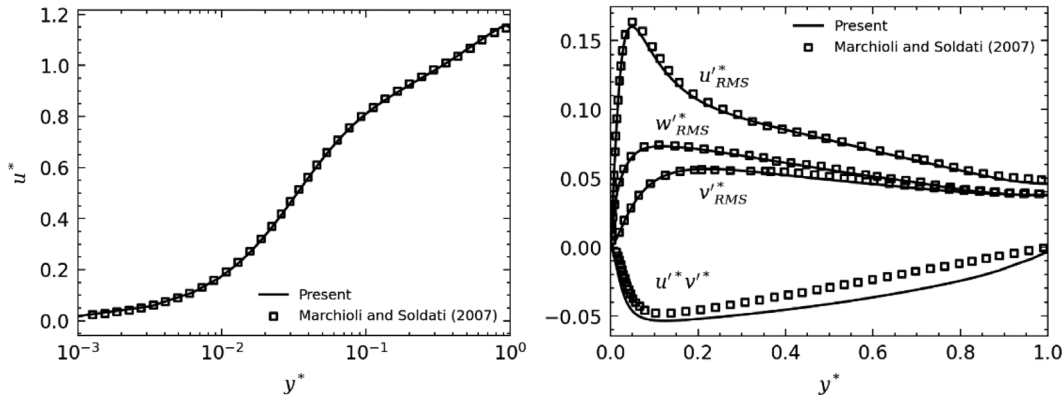
FIG. 4. Profiles of mean fluid streamwise velocity (left) and RMS of velocity fluctuations/shear stress (right) for turbulent channel flow at $Re_\tau = 300$. Findings are compared to Marchioli and Soldati (2007).

interactions are ignored anyway). Each simulation was performed for 20 000 time steps or $t^* = 100$ in bulk scale time units, by which time the particle statistics demonstrated minimal variation with time, although in the cases where turbophoresis was observed, there was still some drift in the concentration field toward the walls. Figure 5 illustrates the mean streamwise particle velocity profiles for both cases. In the bulk flow region, close to the channel center, the Stokes number has a little effect on the resulting statistics, with particles possessing
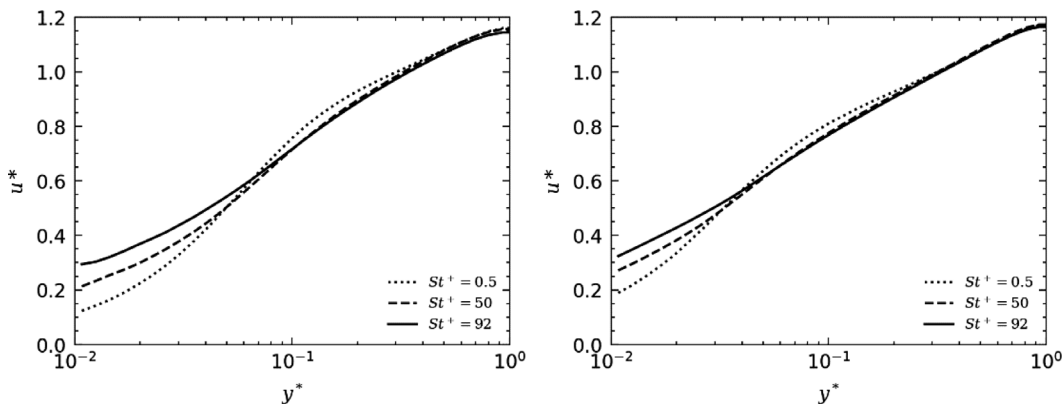

FIG. 5. Mean streamwise particle velocity profiles in one-way coupled turbulent channel flow at $Re_\tau = 180$ (left) and $Re_\tau = 300$ (right). The effect of variation of the particle Stokes number is demonstrated.
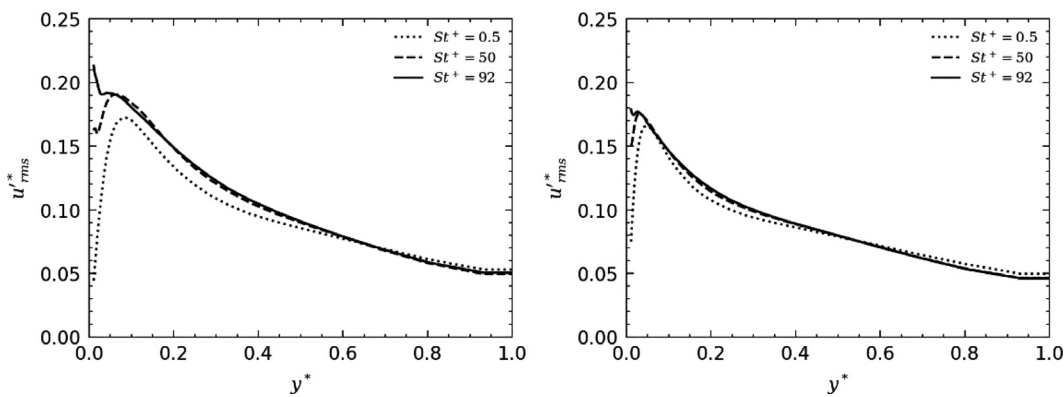

FIG. 6. RMS of streamwise particle velocity fluctuation profiles in one-way coupled turbulent channel flow at $Re_\tau = 180$ (left) and $Re_\tau = 300$ (right). The effect of variation of the particle Stokes number is demonstrated.

similar mean streamwise velocities. However, as the wall is approached, in both cases, low Stokes number particles tend to be faster than their higher density counterparts, with those closer to the wall exhibiting slower behavior.

The RMS of streamwise, wall-normal, and spanwise velocity fluctuations are presented in Figs. 6–8. The streamwise fluctuations exhibit a similar location-based behavior as observed with the mean streamwise velocity, whereby particles close to the channel center possess fluctuations
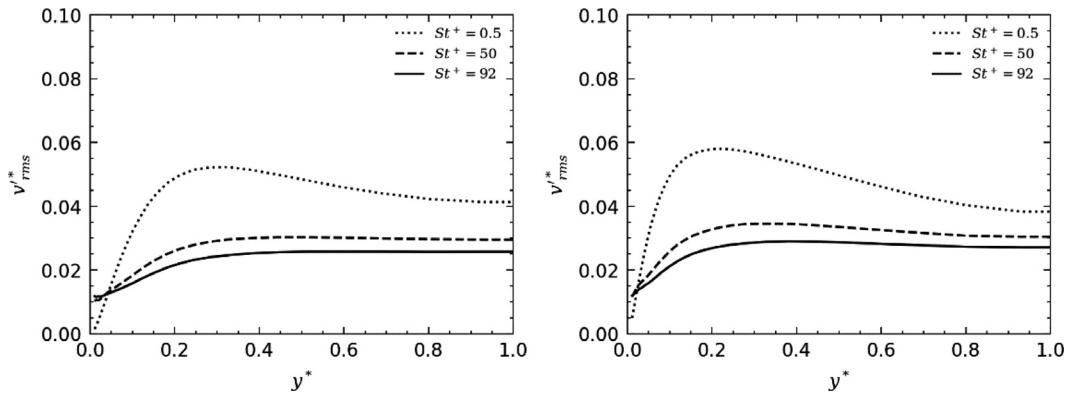

FIG. 7. RMS of wall-normal particle velocity fluctuation profiles in one-way coupled turbulent channel flow at $Re_\tau = 180$ (left) and $Re_\tau = 300$ (right). The effect of variation of the particle Stokes number is demonstrated.
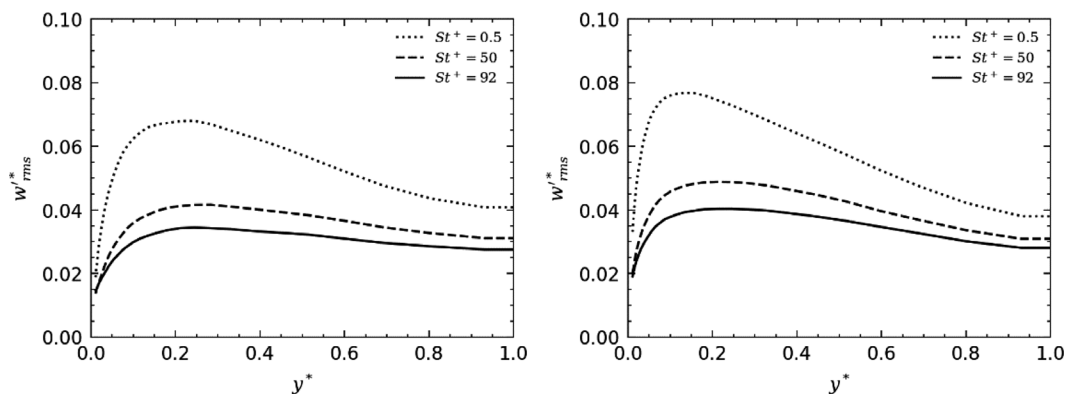

FIG. 8. RMS of spanwise particle velocity fluctuation profiles in one-way coupled turbulent channel flow at $Re_\tau = 180$ (left) and $Re_\tau = 300$ (right). The effect of variation of the particle Stokes number is demonstrated.
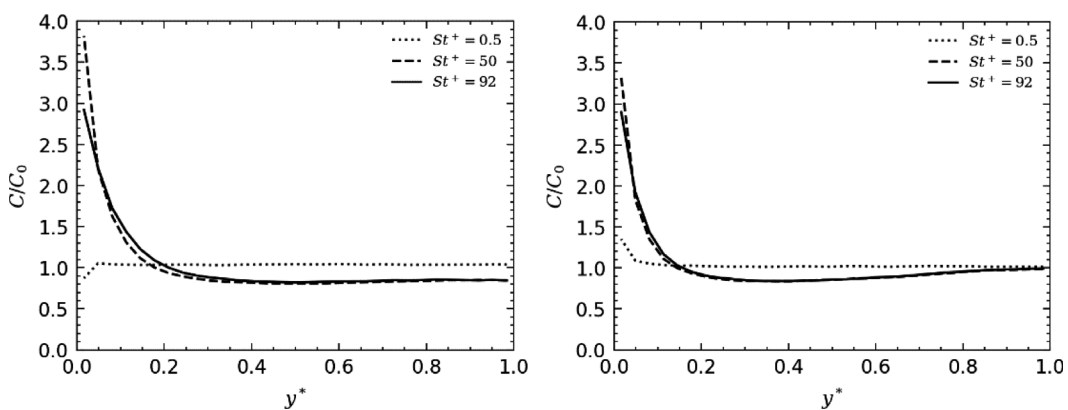

FIG. 9. Particle relative concentration profiles in one-way coupled turbulent channel flow at $Re_\tau = 180$ (left) and $Re_\tau = 300$ (right). The effect of variation of the particle Stokes number is demonstrated.

independent of the Stokes number. Again, as the wall is approached, the behavior bifurcates such that particles with low Stokes numbers exhibit less turbulent motion. For particles very close to the wall, in the viscous sublayer, the motion matches that of the fluid profile for $St = 0.5$ particles. For the two higher Stokes number species, even

though the fluid RMS fluctuations go to zero in that region, particles retain their turbulent motion. This has been studied previously (Mortimer *et al.*, 2019) and is due to inertial particles undergoing sweeping motions toward the wall while retaining their increased velocities from the more turbulent regions such as the buffer and log-law regions.
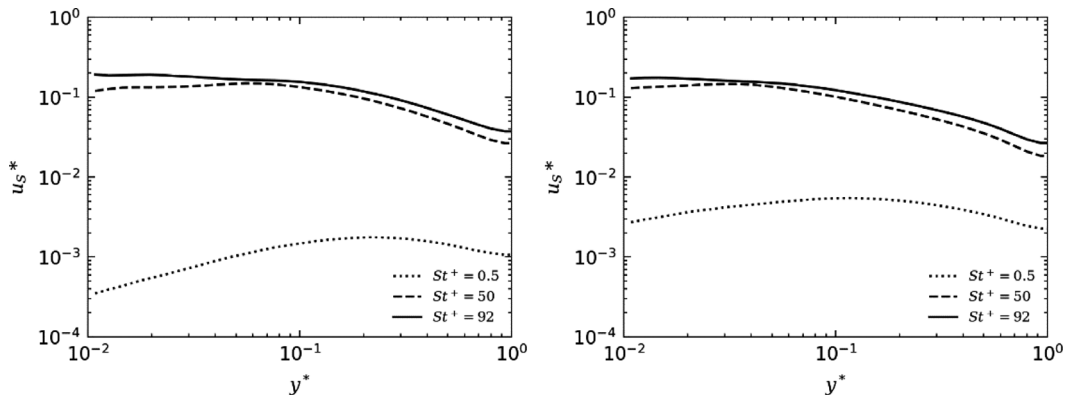

FIG. 10. Mean absolute value of slip velocity profiles in one-way coupled turbulent channel flow at $Re_\tau = 180$ (left) and $Re_\tau = 300$ (right). The effect of variation of the particle Stokes number is demonstrated.
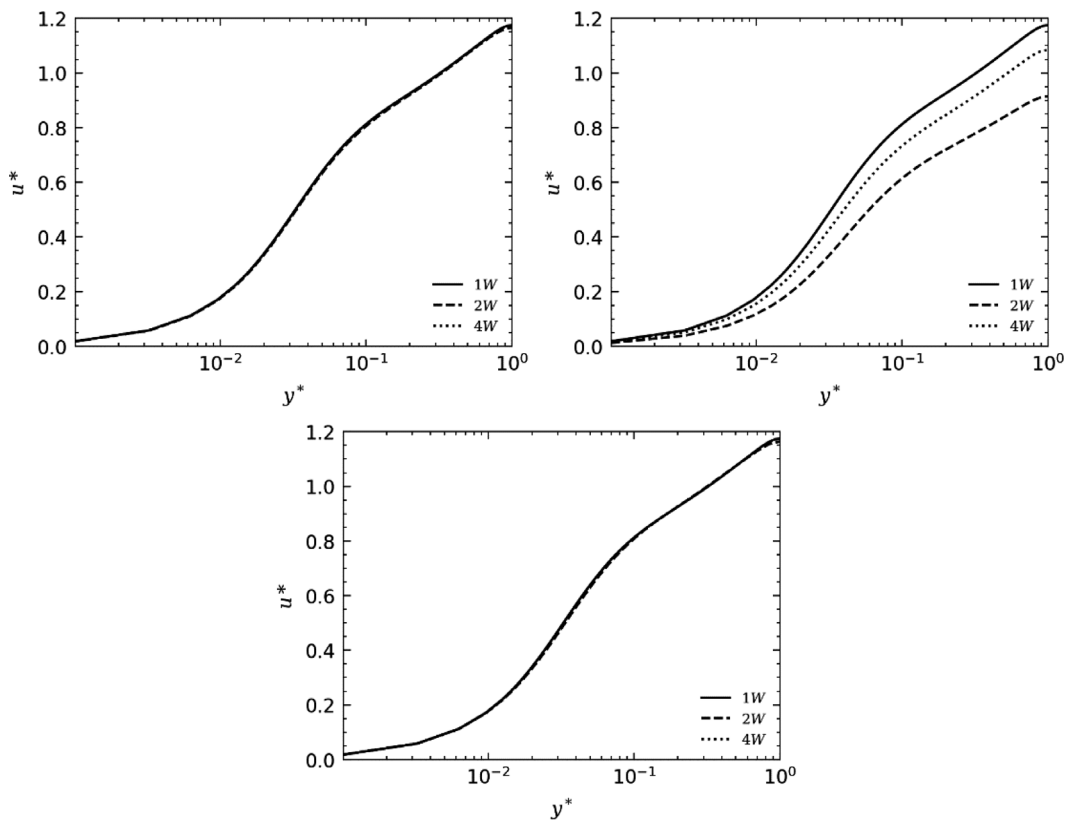

FIG. 11. Mean streamwise fluid velocity profiles in turbulent channel flow at $Re_\tau = 300$ at $St^+ = 0.5$ (upper left), $St^+ = 50$ (upper right), and $St^+ = 92$ (lower). The effect of variation of the coupling method is demonstrated.

At increased Reynolds number, these effects are slightly diminished, likely due to the fact that the turbulence kinetic energy maxima are greater and closer to the wall, meaning that particles reaching these most turbulent regions have already had enough time to be adjust to the local fluid velocity fluctuations. The wall-normal profiles show much more sensitivity to the Stokes number, as do the spanwise profiles, with high Stokes number particles exhibiting dampened turbulent behavior in both directions.

The relative concentration profiles across the wall direction normalized by the initial mean concentration for each particle species are presented in Fig. 9. For the two highest Stokes numbers, the profiles in the bulk remain slightly diminished in favor of increased concentrations close to the wall for both Reynolds number cases. Since the moderate Stokes number, $St^+ = 50$ particle, is closest to the range where preferential concentration has been demonstrated to play a more important role (Eaton and Fessler, 1994; Fessler *et al.*, 1994; and Lee and Lee, 2015), these particles exhibit the maximum wall concentration observed. Notably, the width of the region where the particles begin to congregate is greater for the low Reynolds number case due to the turbulent region, and the region where the turbulence kinetic energy gradient is positive, being narrower for increased Reynolds number. For the lowest Stokes number particles, the concentration profiles remain approximately homogeneous with slight variations close to the wall. It is observed that the increased Reynolds

number case exhibits wall-accumulation for all three particle Stokes numbers, while at $St^+ = 0.5$ in the $Re_\tau = 180$ flow, the particles remain in the bulk flow region. This is likely facilitated again by the fact that the turbulent region is narrower; therefore, it is more likely that a low Stokes number particle in the bulk flow region will penetrate deeper into the turbulent region while retaining an increased velocity from the bulk flow.

In Fig. 10, the mean slip velocity magnitudes are demonstrated across the channel. Due to retention of particle inertia decoupling the particle velocities from those of the fluid, the increased density particles exhibit much higher slip velocities in all cases considered. Similar profiles are observed for the two increased Stokes numbers and at both Reynolds numbers, with the $Re_\tau = 300$ case exhibiting slightly larger slip velocities in the bulk flow region. That said, for these two particle species, the slip velocity profiles are relatively homogeneous where they peak in the turbulent region ($y^* < 0.2$). For the low Stokes particles, the slip velocity is low throughout, demonstrating their adherence to following the fluid streamlines closely, and decreases further both near the channel center and close to the channel wall (where the turbulence kinetic energy reaches its minima). Notably, in the increased Re_τ simulation, the slip velocities of identical St^+ particles are an order of magnitude higher in the turbulent region, further demonstrating their ability to retain their increased velocities as they migrate toward the wall.
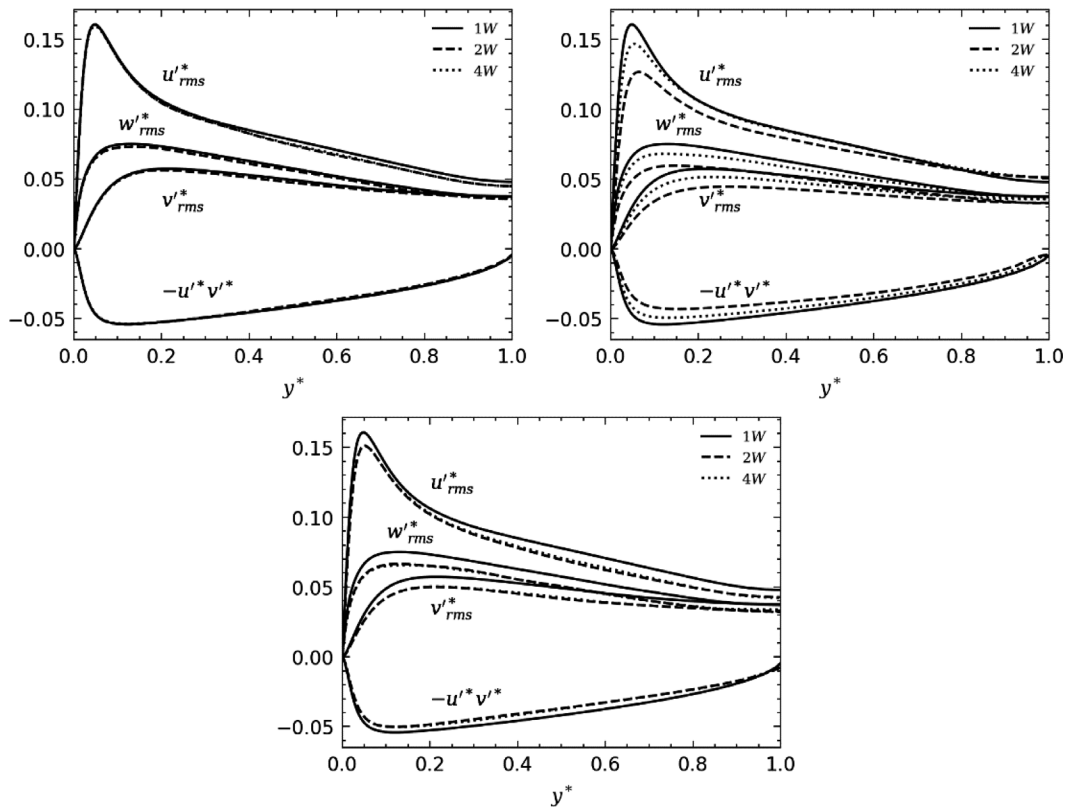

FIG. 12. RMS of velocity fluctuation/shear stress profiles in turbulent channel flow at $Re_\tau = 300$ at $St^+ = 0.5$ (upper left), $St^+ = 50$ (upper right), and $St^+ = 92$ (lower). The effect of variation of the coupling method is demonstrated.

C. Effect of coupling on fluid phase statistics

The effect of the level of coupling between the fluid and particle phases is now studied in the channel flow, keeping the Reynolds number constant at $Re_\tau = 300$ and comparing all three Stokes numbers and all three coupling regimes. Comparisons at $Re_\tau = 180$ indicated similar qualitative results to those present here, and so we choose to focus on the high Reynolds number, which has been less-studied in the literature. In Fig. 11, the effect of coupling on the mean streamwise velocity is studied. As expected, at low Stokes number, $St^+ = 0.5$, the effect is minimal, with only a very slight reduction observed for the two-way coupled simulation. As the Stokes number is increased to $St^+ = 50$, the effects on the fluid phase statistics are much greater. For the two-way coupled simulation, the mean streamwise velocity is reduced, with the greatest reduction taking place at the channel center. This is in line with observations of two-way coupled studies in the literature (Eaton, 2009; Mortimer and Fairweather, 2020), in which this effect has been shown to be strongest for moderate Stokes numbers $St^+ \sim 25$. Interestingly, and standing as a major focus of analysis for this study, the four-way coupled simulation exhibits less reduction in mean streamwise velocity when compared the two-way coupled simulation. For the largest Stokes number considered, there is little variation in the mean streamwise velocity, which again is agreement with the literature (Lee and Lee, 2015), since turbophoresis is reduced beyond moderate Stokes number values and particles are less likely to sample

velocities beyond their local region in the flow due to wall-perpendicular motion.

The RMS of velocity fluctuations for each Stokes number and coupling regime are presented in Fig. 12. Again, for the low Stokes number simulation, there is very little variation with coupling level, though the two-way and four-way coupled systems seem to exhibit some reduction in the streamwise turbulence intensity in the bulk of the channel flow. For the moderate Stokes number, $St^+ = 50$, the two-way system exhibits high turbulence attenuation in all directions, and the shear stresses are also reduced in magnitude. This is well-documented in the literature (Mortimer et al., 2019; Zhao et al., 2015) due to turbophoresis causing inertial particles with memory to migrate perpendicular to the wall whilst retaining their velocities from their initial regions and hence contributing larger slip velocities in their new regions. Again, the four-way coupled simulation exhibits a dampened version of this effect in all three directions. For the highest Stokes number, the two-way and four-way coupled simulations demonstrate agreement indicating that the particle collision dynamics are different for the moderate Stokes number, leading to attenuation of this effect.

D. Effect of coupling on particle phase statistics

To determine the dynamics responsible for this difference between moderate and high Stokes number particles in terms of the effect of two- and four-way coupling, the particulate phase dynamics
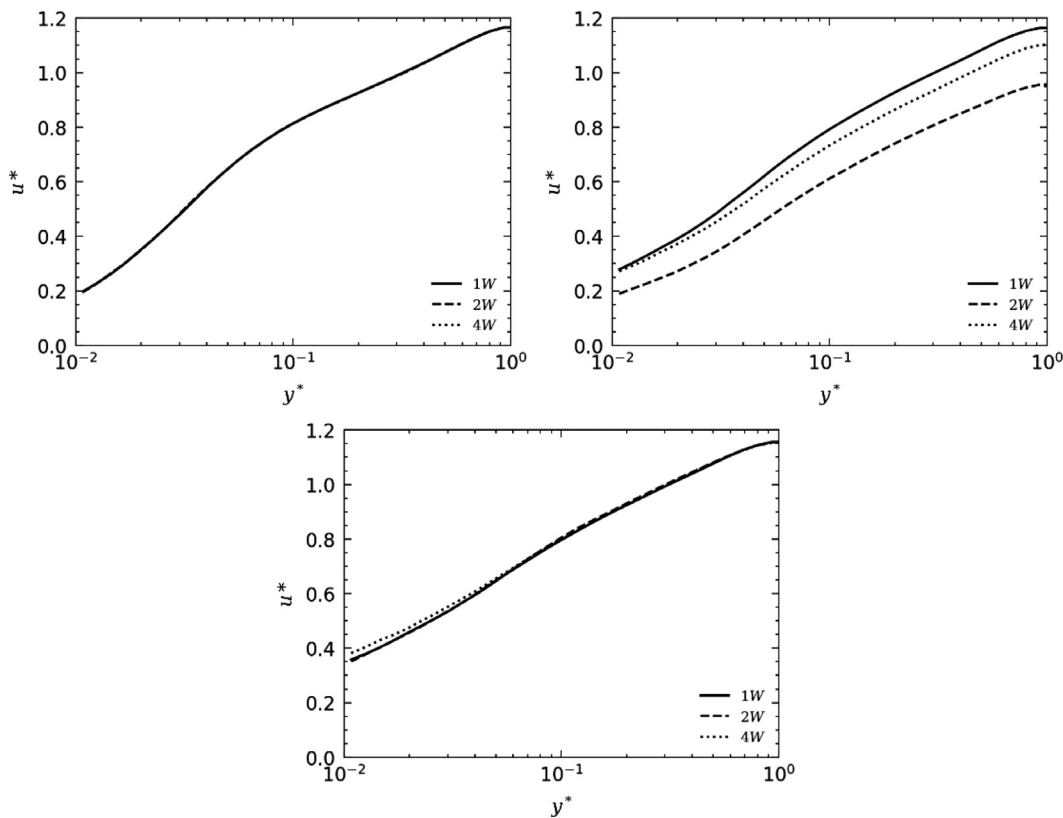

FIG. 13. Mean streamwise particle velocity profiles in turbulent channel flow at $Re_\tau = 300$ at $St^+ = 0.5$ (upper left), $St^+ = 50$ (upper right), and $St^+ = 92$ (lower). The effect of variation of the coupling method is demonstrated.
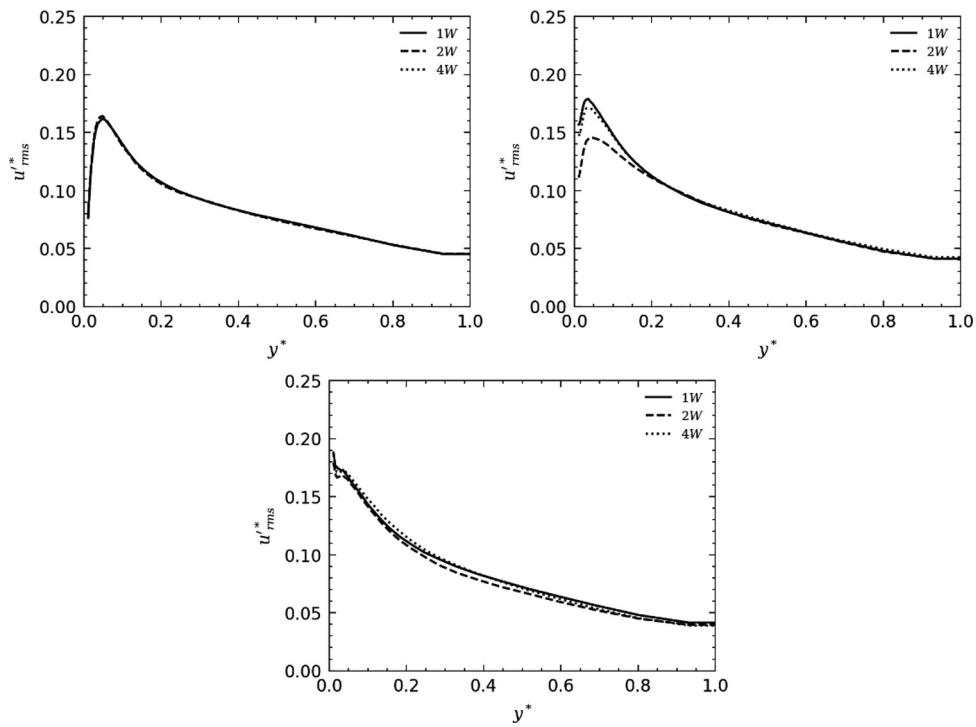
FIG. 14. RMS of streamwise particle velocity fluctuation profiles in turbulent channel flow at $Re_\tau = 300$ at $St^+ = 0.5$ (upper left), $St^+ = 50$ (upper right), and $St^+ = 92$ (lower). The effect of variation of the coupling method is demonstrated.

FIG. 15. RMS of wall-normal particle velocity fluctuation profiles in turbulent channel flow at $Re_\tau = 300$ at $St^+ = 0.5$ (upper left), $St^+ = 50$ (upper right), and $St^+ = 92$ (lower). The effect of variation of the coupling method is demonstrated.
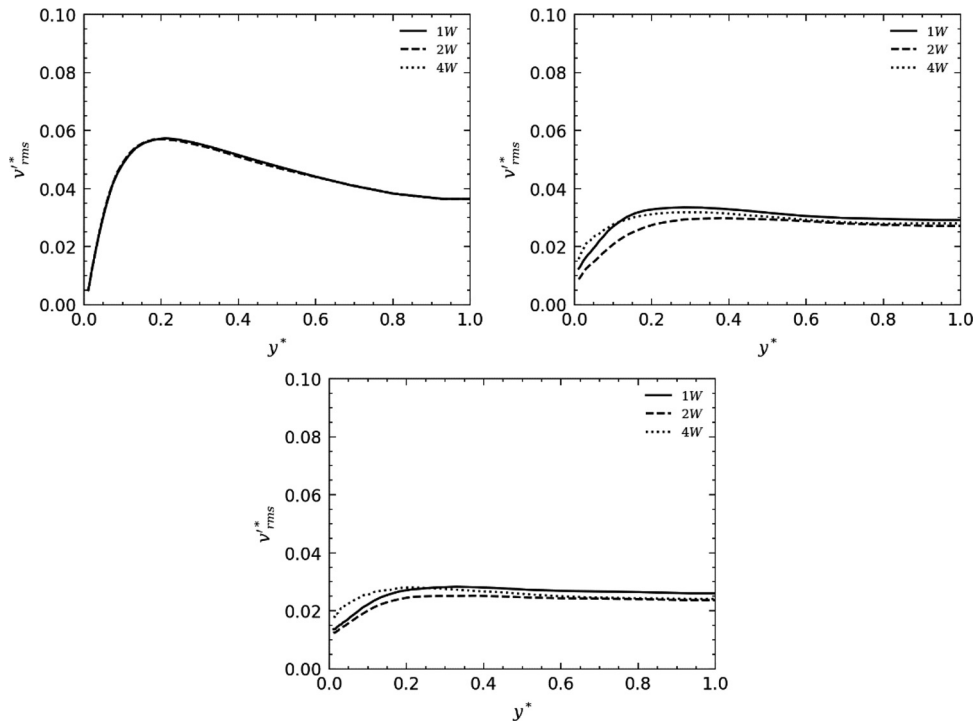
are studied. In Fig. 13, the particle mean streamwise velocities are presented for each Stokes number and coupling regime. For the low ($St^+ = 0.5$) and high ($St^+ = 92$) Stokes number particles, the mean streamwise velocities are largely unaffected by the level of coupling, with only slight variations exhibited in the near-wall region of the high Stokes number case, where the four-way coupled simulation shows particles with increased velocities. Conversely, it is observed in the moderate Stokes number case that particle velocities are reduced throughout the channel flow when two-way coupled, an effect that is dampened again when collisions are also considered. This is in line with the results of Fig. 11, in that the fluid phase also slows down depending on the coupling level. Notably, as the wall is approached, the profiles for the one- and four-way coupled approaches converge. It is, therefore, implied that the existence of particle collisions modifies the way in which the particles feedback their force on to the fluid, and that in the viscous sublayer this effect is strongest. In Fig. 14, the streamwise RMS velocities for the particulate phase are presented. Again, very little variation with coupling level is observed for the low and high Stokes number simulations. Interestingly, in the bulk flow region ($y^* > 0.2$), even at the moderate Stokes number, all three coupling regimes demonstrate almost identical behavior considering streamwise particle turbulence intensities, despite the fluid exhibiting different characteristics. In the turbulent region, the streamwise fluctuations are reduced somewhat for the two-way coupled simulation, but restored in the four-way coupled predictions, indicating again that the

collisions are capable of modifying the dynamics leading to turbulence attenuation in this region. The wall-normal particle velocity fluctuations (Fig. 15) offer more insight. Again, at low Stokes number, they are unmodified by coupling regime, and in the two-way coupled simulation at moderate and high Stokes numbers, the fluctuations are dampened throughout. For the four-way coupled simulations, it appears that the presence of collisions reduces the fluctuations in the bulk flow but increases them close to the wall. It can be ascertained that the collisions taking place close to the wall redistribute the streamwise momentum in the wall-normal direction.

Similarly, in Fig. 16, the spanwise RMS of the particle velocity fluctuations exhibit similar behavior, though the redistribution to this direction takes place more so in the $St^+=92$ simulation. In all cases, the presence of inertial collisions decoupling the particle velocities from the local flow velocity leads to increased fluctuations, an effect that is strongest for the moderate Stokes number and also in the turbulent regions of the flow.

This can be investigated further by studying where the particles are concentrated in each system, which will govern the chance for collisions to take place, as well as contributing to the magnitude of the two-way coupling feedback force. The concentration profiles are presented in Fig. 17. For the low Stokes number simulation, the coupling level has a negligible effect on the distribution of particles throughout the channel flow. This is due to the two-way coupling forces being very low due to small slip velocities, which also means that particle
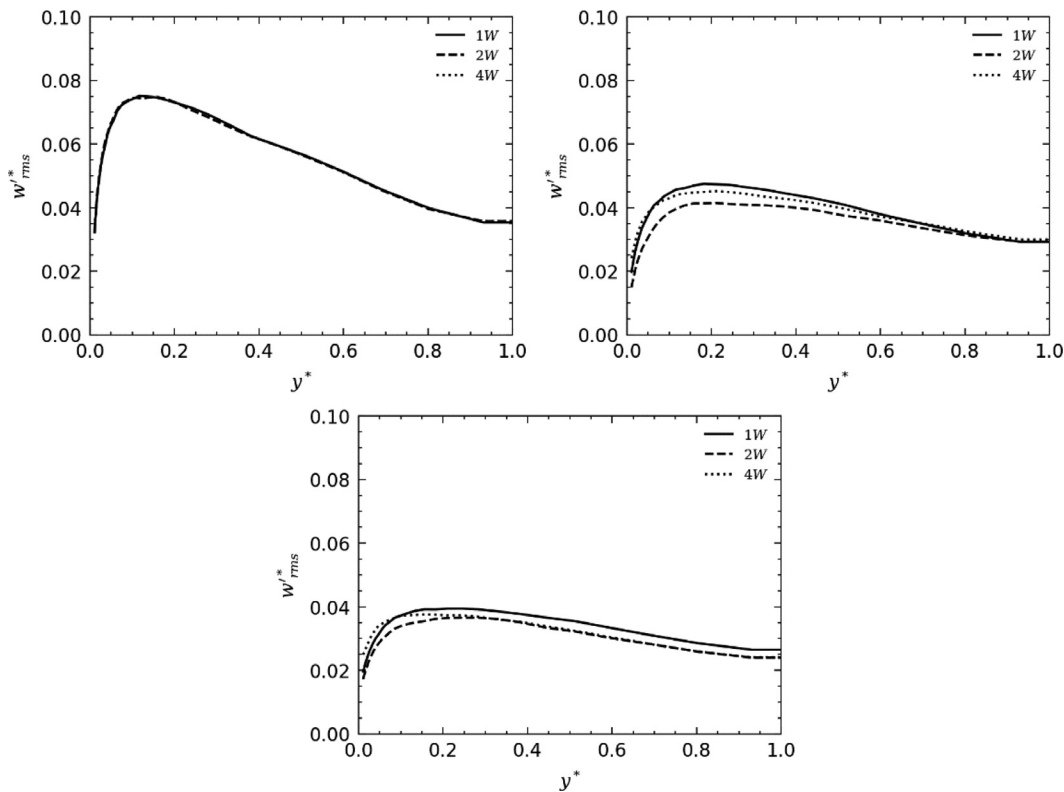

FIG. 16. RMS of spanwise particle velocity fluctuation profiles in turbulent channel flow at $Re_\tau = 300$ at $St^+ = 0.5$ (upper left), $St^+ = 50$ (upper right), and $St^+ = 92$ (lower). The effect of variation of the coupling method is demonstrated.

FIG. 17. Particle relative concentration profiles in turbulent channel flow at $Re_\tau = 300$ at $St^+ = 0.5$ (upper left), $St^+ = 50$ (upper right), and $St^+ = 92$ (lower). The effect of variation of the coupling method is demonstrated.
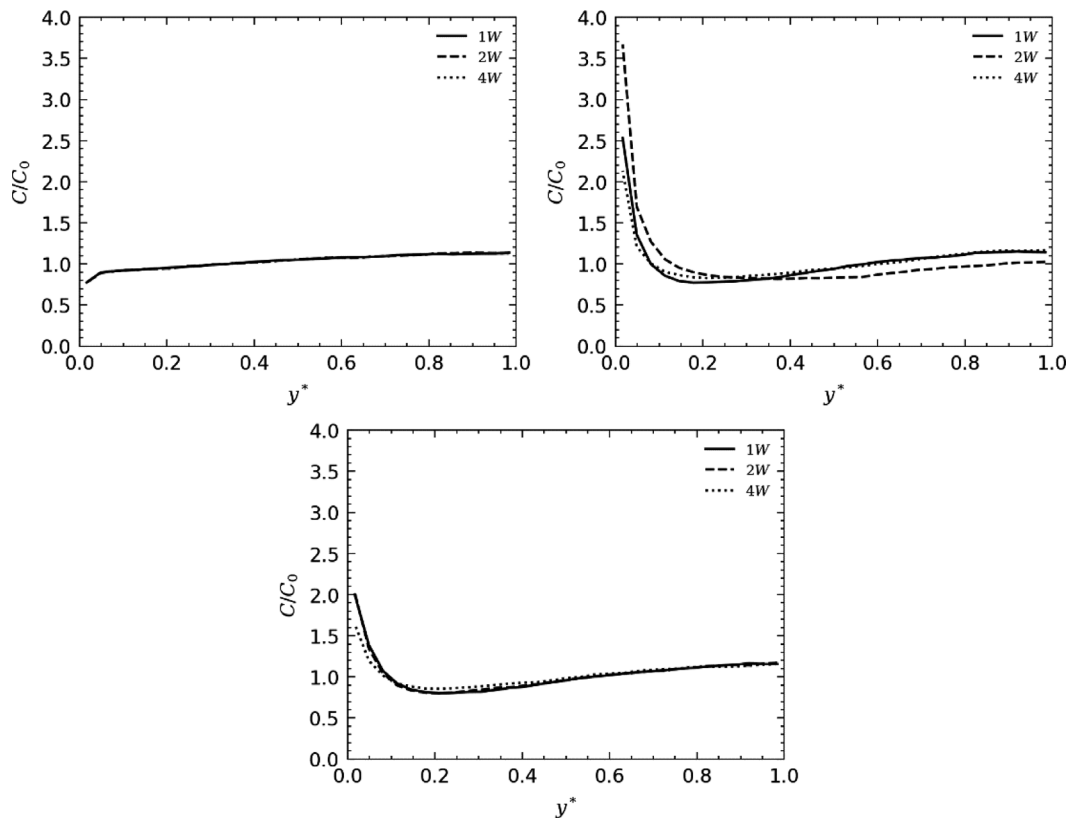
collisions will take place between pairs of particles in local fluid regions which will very likely possess similar momenta, and hence, any redistribution will be very small and soon recovered due to the low particle timescale. At moderate Stokes number, two-way coupling causes a large increase in the near-wall particle concentration, with particles being removed from the bulk flow in favor of this region. The two-way coupling effects increase the extent of turbophoresis. This could be due to a modification in the shear Reynolds number and hence the fluid timescale causing the particulate timescale to more closely match that in the region where turbophoresis is dominant. Interestingly, with collisions having already been demonstrated to dampen the effect of two-way coupling, this leads to a reduction in particle concentration near the wall, with intermediate collisions interfering with the wall-perpendicular migration. For the largest Stokes number, the one- and two-way coupled simulations demonstrate almost identical profiles for particle concentration, whereas the presence of collisions once again hinders the migration leading to fewer particles in the near-wall region.

Since the slip velocity also governs the extent of particle–fluid feedback, we consider the variation of the mean magnitude of this quantity in Fig. 18. Again, negligible differences are observed for the low Stokes particles, which, combined with Fig. 17, explains the miniscule effects on the fluid flow observed in Figs. 11 and 12. For the moderate Stokes number particle, the slip velocities are reduced throughout

for the two-way coupled simulation, with the greatest effects observed close to the wall. Four-way coupling once again dampens these effects, leading to slip velocities more closely resembling those in the one-way coupled simulation. When particles and the surrounding fluid exchange momenta, the slip velocity will be reduced due to their velocities approaching one another. In the case with collisions, among this momenta exchange, there will exist events where the particles suddenly redirect their momentum, leading to a decoupling of their velocity from the local fluid. This effect does not seem to take place in the high Stokes number simulation, indicating that turbophoresis is a critical factor for this phenomenon, and implying that collision due to wall-normal migration of particles is a key contributing factor for these diminishing two-way coupling effects.

E. Effect of coupling on particle phase velocity distributions

In this subsection, it is investigated how the coupling regime affects the distribution of velocities in various regions of the flow in order to ascertain the responsible dynamics leading to collisions that reduce the effects of two-way coupling for moderate Stokes number particles. Figure 19 illustrates the probability distribution functions (PDFs) for particle streamwise velocity in each wall-normal channel flow region. The distributions are unaffected by the coupling regime
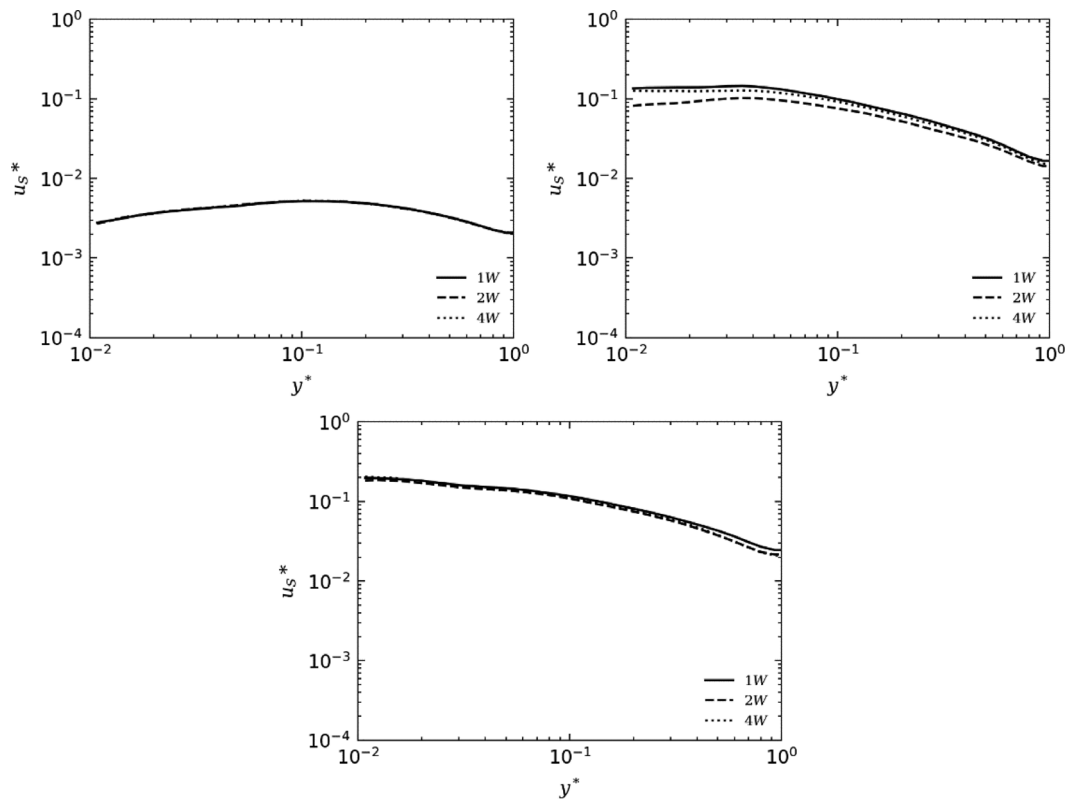
FIG. 18. Mean absolute value of slip velocity profiles in turbulent channel flow at $Re_\tau = 300$ at $St^+ = 0.5$ (upper left), $St^+ = 50$ (upper right), and $St^+ = 92$ (lower). The effect of variation of the coupling method is demonstrated.

for the $St^+ = 0.5$ particles, as expected, and are very similar for the high Stokes number particles as well, with only minor variations observed. For the moderate Stokes number particles, the velocities are reduced with two-way coupling, though the inclusion of interparticle collisions leads to their profiles moving closer to those of the one-way coupled flow, with the greatest recovery of velocity for the profiles closest to the wall.

In Fig. 20, the wall-normal velocity PDFs are compared for each Stokes number and coupling level. Again, the low Stokes number simulations indicate negligible differences between the coupling levels. In the two-way coupled simulation, similar observations are made as in Fig. 19, where the near-wall regions exhibit very similar behavior between the one-way and four-way coupled simulations. Interestingly, the log-law region shows four-way coupled particles with velocity distributions closer to those of the two-way than the one-way coupled simulations, consistent with the overlap in Fig. 15. It is implied that beyond the log-law region, the collision behavior begins to contribute to the increase in wall-normal fluctuations. This could be due to collisions with the wall, reversing the velocities in the wall-normal direction, as well as the frequent collisions in this region caused by preferential concentration. The dynamics of these collisions which may lead to this redistribution of momenta are studied in Subsection III.F. Considering the largest Stokes number, the two- and four-way coupled simulations exhibit similar behavior, with the log-law region

demonstrating agreement. The spanwise velocity presented in Fig. 21 indicates similar observations, though the strongest agreement between the two- and four-way coupled simulations is found in the log-law region of the $St^+ = 92$ system.

Particle slip velocity PDFs are also compared in Fig. 22, with negligible variation of this quantity observed in the low Stokes number system. Analysis into the presence of the bumps around $|u_S^*| = 0.02$ indicated that these were particles moving to regions of low fluid velocity (i.e., low speed streaks) which leads to a slight increase in slip velocities equivalent to the difference between the velocities of the streaks and the surrounding fluid. For $St^+ = 50$, all three coupling regimes demonstrate similar distributions for high slip velocities, whereas for low slip velocities, the four-way coupled distributions more closely resemble those of the one-way coupled system. Interestingly, in the $St^+ = 92$ system, the two-way and four-way coupled flows demonstrate agreement in all regions aside from the viscous sublayer (where collisions are much more likely and prone to skew the distribution toward increased slip velocities), further implying that these effects are present only for the moderate Stokes number particles.

F. Particle collision dynamics

Finally, the distribution and properties of collisions are discussed throughout the channel flow in context to their effects on the
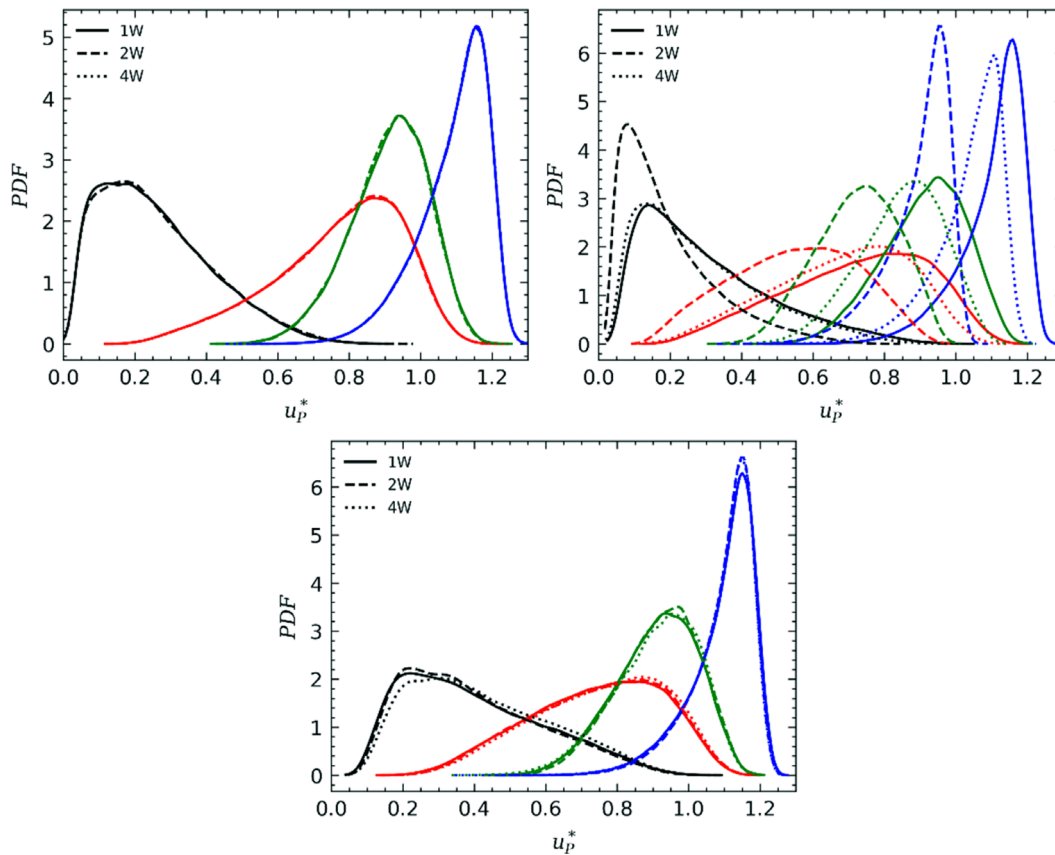
FIG. 19. PDFs of particle streamwise velocity in channel flow regions at $St^+ = 0.5$ (upper left), $St^+ = 50$ (upper right), and $St^+ = 92$ (lower). Black: viscous sublayer; red: buffer layer; green: log-law region; blue: bulk flow.

particle–fluid feedback force and slip velocities. The left plot in Fig. 23 illustrates the total number of collisions occurring throughout the channel flow for each Stokes number particle species studied. At $St^+ = 0.5$, collisions are approximately homogeneous throughout the channel, with previous studies (Mortimer *et al.*, 2020) indicating streamwise orientated collisions as one particle collides with one ahead of it at very low relative collision angle and velocity. At high Stokes number, collisions become more frequent close to the wall, where retained momentum from regions closer to the bulk lead to particles crossing streamlines and quasi-streamwise vortices where other particles may reside. The wall collision frequency peaks for the moderate Stokes number, which is likely due to both preferential concentration and turbophoresis where particles migrating toward the bulk flow region will hit those that are moving more slowly in low-speed streaks. If we compare this profile to the relative increase in mean streamwise velocity between the four-way and two-way coupled systems, it is clear that the variation correlates well with the collision event density close to the wall, further confirming that the collision dynamics lead to a suppression of the two-way coupling feedback force.

To determine the dynamics of such collisions, PDFs of relative collision velocity magnitude and angle are presented in Figs. 24 and 25. For the lowest Stokes number particles, both relative velocities and angles are low, with a slight increase in those taking place within the viscous sublayer, confirming that these types of collisions are advective in that they occur as one particle follows a fluid streamline behind another. As the Stokes number is increased, at $St^+ = 50$, the relative velocity of the collisions also increases, with collisions within the wall-regions exhibiting more ballistic behavior. Relative collision angles in all three near-wall regions are similar, and greater than those present in the bulk flow region. Collisions occurring with high initial relative velocities and at larger angles will result in greater directional impulses leading to a redistribution of momentum which explains the increases in slip velocity observed in the four-way coupled flows (Fig. 22). The velocities and angles for collisions occurring with the $St^+ = 92$ particles are similar to those observed at $St^+ = 50$, though the number of collisions occurring throughout the flow is lower, hence, the magnitude of the suppression of the two-way feedback force effect is lower.

Collisions between particles where the relative velocity is high will result in the greatest transfer of momentum and hence decoupling from the local fluid velocity field. In Fig. 26, the collider velocities are plotted with color indicating the region the collision took place in. We further confirm that for $St^+ = 0.5$, the collision constituents possess very similar velocities in all regions of the channel flow, with only minor deviations beyond the log-law region. In fact, as the Stokes
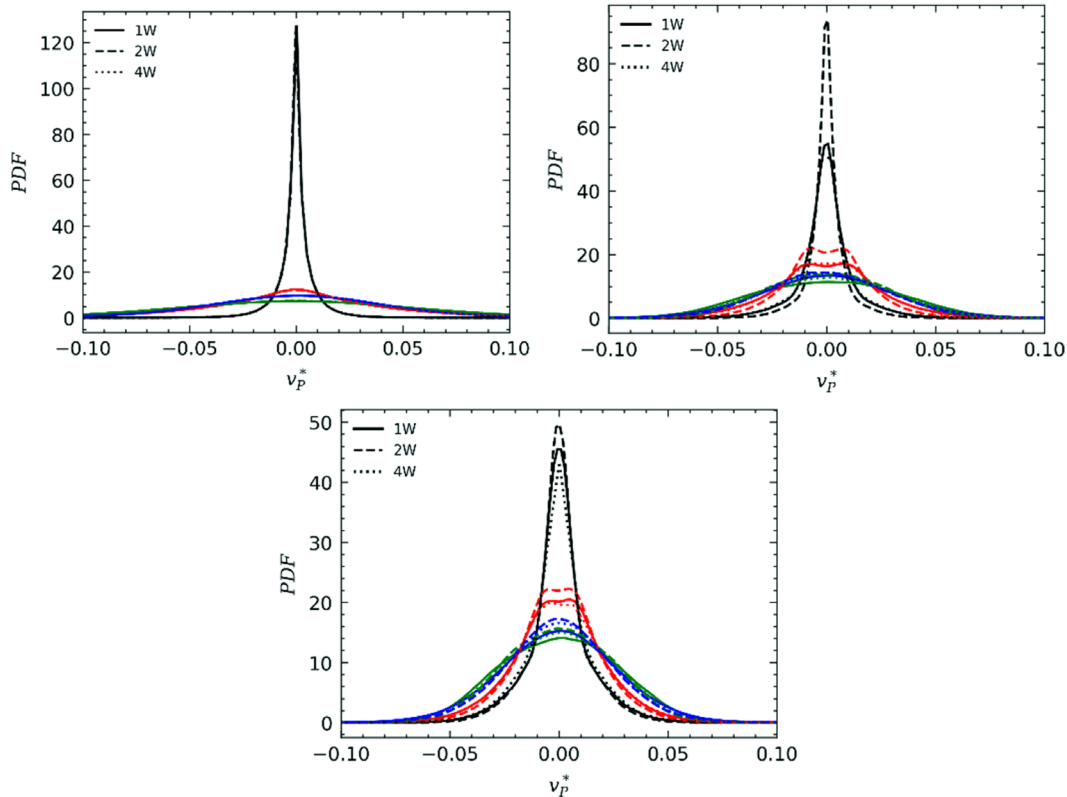
FIG. 20. PDFs of particle wall-normal velocity in channel flow regions at $St^+ = 0.5$ (upper left), $St^+ = 50$ (upper right), and $St^+ = 92$ (lower). Black: viscous sublayer; red: buffer layer; green: log-law region; blue: bulk flow.

number is increased, we observe that collisions between similar velocity particles are more unlikely outside of the bulk flow region, with more collisions occurring between particle of differing velocities close to the channel wall. This trend is repeated for the $St^+ = 92$ particles, although the number of collisions is low, weakening the effect of suppression of two-way coupling feedback forces.

IV. CONCLUSIONS AND OUTLOOK

In this study, the effect of flow Reynolds number ($Re_\tau = 180, 300$), particle Stokes number ($St^+ = 0.5, 50,$ and 92), and fluid–particle coupling level (one-way, two-way, and four-way) on particle behavior have been investigated. Direct numerical simulation of particle-laden turbulent channel flows alongside Lagrangian particle tracking was used to predict the continuous phase, as well as the trajectories of dispersed particles, taking into account force-feedback onto the fluid as well as interparticle collisions.

After demonstrating excellent validation of the single-phase predictions against previous DNS studies, the effect of Reynolds number on one-way coupled particle statistics was considered across three Stokes numbers accounting for low ($St^+ = 0.5$), moderate ($St^+ = 50$), and high ($St^+ = 92$) values. It was found that as the Reynolds number is increased, due to the thinner turbulent region, the effects where particles retain their velocity through wall-normal sweep events diminish, leading to reduced near-wall RMS streamwise velocity fluctuations.

This also leads to reduced preferential concentration in the wall-region, though evidence is observed that even the low Stokes particles begin to accumulate in the $Re_\tau = 300$ simulation, whereas in the $Re_\tau = 180$ simulation, they are depleted close to the wall. Considering the effect of coupling on the particle behavior in the $Re_\tau = 300$ simulation yields some interesting findings. For moderate Stokes numbers, the four-way coupled flow exhibits similar statistics for both the particulate and continuous phase to that of the one-way coupled flow, with the two-way coupled system predicting greater feedback forces from the particle phase. This is not observed for the low or high Stokes number particles, and therefore, it is likely that this effect is due to the increased turbophoresis and preferential concentration associated with midrange Stokes numbers. By studying the particle phase collision statistics, it is found that the suppression of the two-way coupling effects is found in those regions where collisions most commonly occur. Furthermore, these collisions possess the highest relative velocities and angles, leading to increased momentum transfer and reorientation, modifying the way in which the particles impart their feedback force back to the fluid.

Overall, the decision to attempt to improve simulations through the inclusion of two-way coupling without also accounting for interparticle collisions, as warranted at sufficient volume fractions, has been shown to actually weaken the accuracy of the results. The three Stokes numbers considered encompass particle behavior in the three key
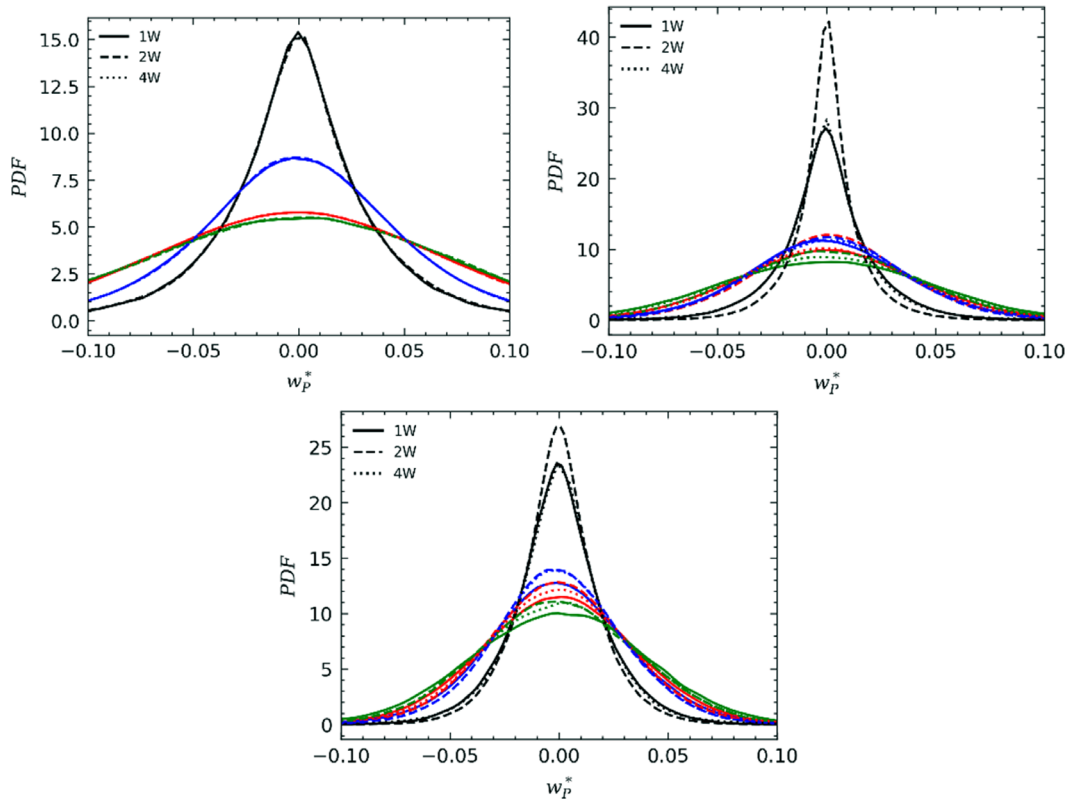
FIG. 21. PDFs of particle spanwise velocity in channel flow regions at $St^+ = 0.5$ (upper left), $St^+ = 50$ (upper right), and $St^+ = 92$ (lower). Black: viscous sublayer; red: buffer layer; green: log-law region; blue: bulk flow.
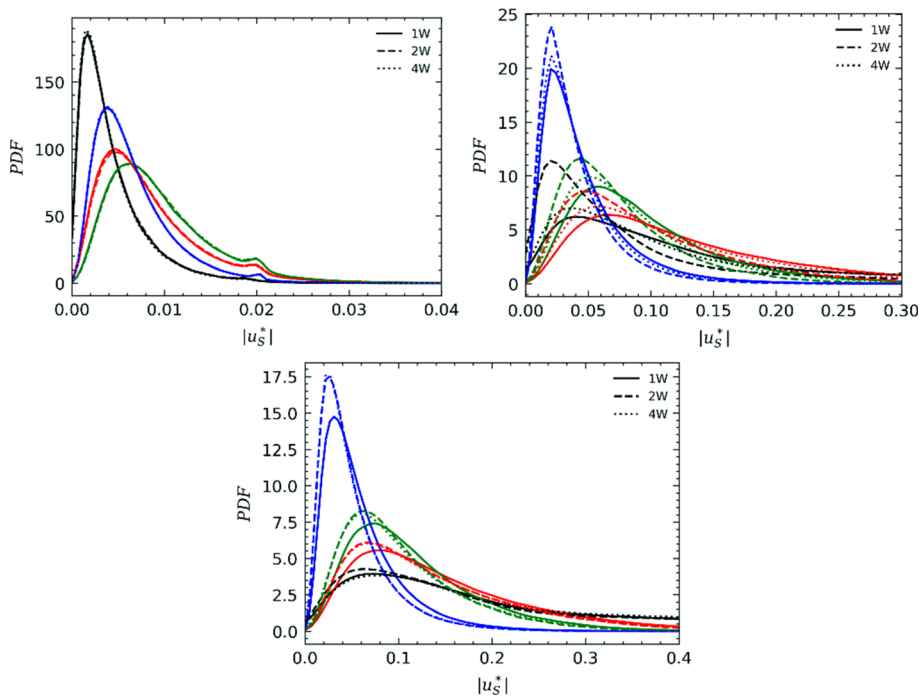

FIG. 22. PDFs of particle slip velocity in channel flow regions at $St^+ = 0.5$ (upper left), $St^+ = 50$ (upper right), and $St^+ = 92$ (lower). Black: viscous sublayer; red: buffer layer; green: log-law region; blue: bulk flow.
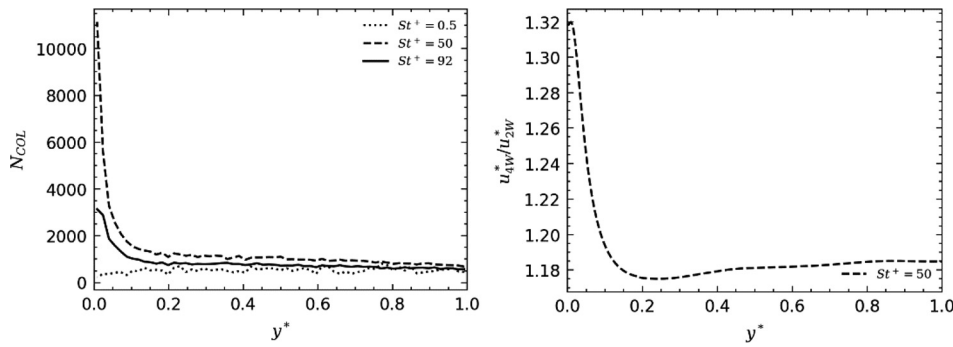
FIG. 23. Total number of collisions across the wall-normal direction (left) and relative change in the mean streamwise velocity as coupling level is increased from two-way to four-way (right). The effect of the Stokes number is illustrated in the left plot.
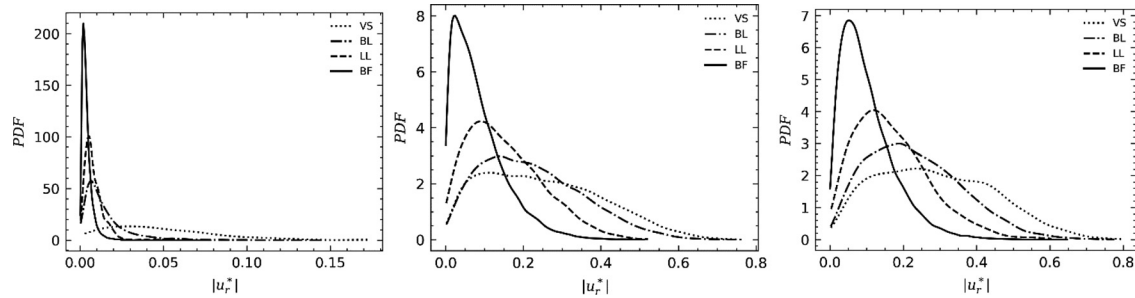

FIG. 24. PDFs of the relative collision velocity magnitude in channel flow regions at $St^+ = 0.5$ (upper left), $St^+ = 50$ (upper right), and $St^+ = 92$ (lower).
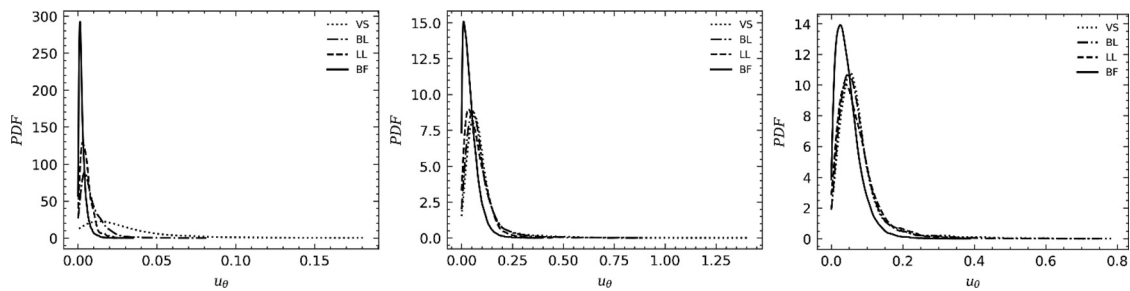

FIG. 25. PDFs of relative collision angle in channel flow regions at $St^+ = 0.5$ (upper left), $St^+ = 50$ (upper right), and $St^+ = 92$ (lower).
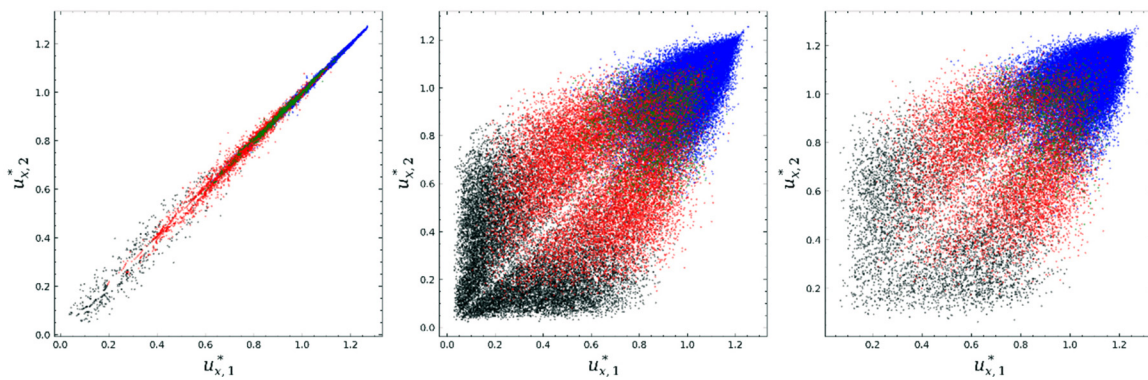

FIG. 26. Collision velocities for particle pairs at $St^+ = 0.5$ (left), $St^+ = 50$ (middle), and $St^+ = 92$ (right). Black: viscous sublayer; red: buffer layer; green: log-law region; blue: bulk flow.

regimes (tracer-like, turbophoresis-driven, and high inertia). We have demonstrated that the particle–fluid interaction hindering effect is strongest, and hence related to, Stokes numbers at which turbophoretic drift and preferential concentration are dominant, and as such the behavior is likely to exist for particle species with Stokes numbers also in this range. The effect of particle concentration is likely also to play an important role for even low and high Stokes numbers, since the collision frequency will increase and hence so will the impact on the direction and magnitude of the fluid feedback force.

ACKNOWLEDGMENTS

AUTHOR DECLARATIONS
Conflict of Interest

The authors have no conflicts to disclose.

Author Contributions

David Rupp: Conceptualization (equal); Data curation (equal); Formal analysis (equal); Investigation (equal); Methodology (equal); Project administration (equal); Resources (equal); Validation (equal); Visualization (equal); Writing – original draft (equal); Writing – review & editing (equal). **Lee Mortimer:** Conceptualization (equal); Data curation (equal); Formal analysis (equal); Investigation (equal); Methodology (equal); Project administration (equal); Software (equal); Supervision (equal); Validation (equal); Visualization (equal); Writing – original draft (equal); Writing – review & editing (equal). **Michael Fairweather:** Conceptualization (equal); Funding acquisition (equal); Project administration (equal); Resources (equal); Supervision (equal); Writing – original draft (equal); Writing – review & editing (equal).

DATA AVAILABILITY

The data that support the findings of this study are available from the corresponding author upon reasonable request.

REFERENCES

M. A. Allison, B. T. Yuill, E. A. Meselhe, J. K. Marsh, A. S. Kolker, and A. D. Ameen, "Observational and numerical particle tracking to examine sediment dynamics in a Mississippi River delta diversion," Estuarine, Coastal Shelf Sci. **194**, 97–108 (2017).

M. Boivin, O. Simonin, and K. D. Squires, "Direct numerical simulation of turbulence modulation by particles in isotropic turbulence," J. Fluid Mech. **375**, 235–263 (1998).

M. Breuer and N. Almohammed, "Modeling and simulation of particle agglomeration in turbulent flows using a hard-sphere model with deterministic collision detection and enhanced structure models," Int. J. Multiphase Flow **73**, 171–206 (2015).

M. Chen, K. Kontomaris, and J. B. McLaughlin, "Direct numerical simulation of droplet collisions in a turbulent channel flow. Part I: Collision algorithm," Int. J. Multiphase Flow **24**, 1079–1103 (1999).

C. J. Cunliffe, J. M. Dodds, and D. J. Dennis, "Flow correlations and transport behaviour of turbulent slurries in partially filled pipes," Chem. Eng. Sci. **235**, 116465 (2021).

A. Daitche, "On the role of the history force for inertial particles in turbulence," J. Fluid Mech. **782**, 567–593 (2015).

C. D. Dritselis, "Direct numerical simulation of particle-laden turbulent channel flows with two-and four-way coupling effects: Budgets of Reynolds stress and streamwise enstrophy," Fluid Dyn. Res. **48**, 015507 (2016).

J. K. Eaton, "Two-way coupled turbulence simulations of gas-particle flows using point-particle tracking," Int. J. Multiphase Flow **35**, 792–800 (2009).

J. K. Eaton and J. Fessler, "Preferential concentration of particles by turbulence," Int. J. Multiphase Flow **20**, 169–209 (1994).

S. Elghobashi, "On predicting particle-laden turbulent flows," Appl. Sci. Res. **52**, 309–329 (1994).

S. Elghobashi, "Direct numerical simulation of turbulent flows laden with droplets or bubbles," Annu. Rev. Fluid Mech. **51**, 217–244 (2019).

M. Fairweather and J. P. Hurn, "Validation of an anisotropic model of turbulent flows containing dispersed solid particles applied to gas-solid jets," Comput. Chem. Eng. **32**, 590–599 (2008).

J. R. Fessler, J. D. Kulick, and J. K. Eaton, "Preferential concentration of heavy particles in a turbulent channel flow," Phys. Fluids **6**, 3742–3749 (1994).

P. F. Fischer, J. W. Lottes, and S. G. Kerkemeier, see http://nek5000.mcs.anl.gov/ for "Nek5000;" accessed 1 September 2008.

H. Homann and J. Bec, "Finite-size effects in the dynamics of neutrally buoyant particles in turbulent flow," J. Fluid Mech. **651**, 81–91 (2010).

R. P. B. Hoomans, J. A. M. Kuipers, W. J. Briels, and W. P. M. van Swaaij, "Discrete particle simulation of bubble and slug formation in a two-dimensional gas-fluidised bed: A hard-sphere approach," Chem. Eng. Sci. **51**, 99–118 (1996).

P. J. Ireland, A. D. Bragg, and L. R. Collins, "The effect of Reynolds number on inertial particle dynamics in isotropic turbulence. Part 1. Simulations without gravitational effects," J. Fluid Mech. **796**, 617–658 (2016).

J. G. M. Kuerten and A. Vreman, "Can turbophoresis be predicted by large-eddy simulation?," Phys. Fluids **17**, 011701 (2005).

S. Laín, M. Sommerfeld, and J. Kussin, "Experimental studies and modelling of four-way coupling in particle-laden horizontal channel flow," Int. J. Heat Fluid Flow **23**, 647–656 (2002).

J. Lee and C. Lee, "Modification of particle-laden near-wall turbulence: Effect of Stokes number," Phys. Fluids **27**, 023303 (2015).

H. Lee and W. Hwang, "Prediction of homogeneous isotropic turbulence modulation by small and heavy particles," Phys. Fluids **34**, 081703 (2022).

M. Liu, Y. Zhao, Y. Yan, M. Fairweather, and J. Yao, "Particle behavior in a turbulent pipe flow with a flat bed," Particuology **81**, 58–72 (2023).

F. Lucci, A. Ferrante, and S. Elghobashi, "Is Stokes number an appropriate indicator for turbulence modulation by particles of Taylor-length-scale size?," Phys. Fluids **23**, 025101 (2011).

C. Marchioli and A. Soldati, "Mechanisms for particle transfer and segregation in a turbulent boundary layer," J. Fluid Mech. **468**, 283–315 (2002).

C. Marchioli and A. Soldati, "Reynolds number scaling of particle preferential concentration in turbulent channel flow," in Advances in Turbulence XI (Springer, 2007), pp. 298–300.

C. Marchioli, A. Soldati, J. G. M. Kuerten, B. Arcen, A. Taniere, G. Goldensoph, K. D. Squires, M. F. Cargnelutti, and L. M. Portela, "Statistics of particle dispersion in direct numerical simulations of wall-bounded turbulence: Results of an international collaborative benchmark test," Int. J. Multiphase Flow **34**, 879–893 (2008).

M. R. Maxey, "The motion of small spherical particles in a cellular flow field," Phys. Fluids **30**, 1915–1928 (1987).

L. F. Mortimer and M. Fairweather, "Density ratio effects on the topology of coherent turbulent structures in two-way coupled particle-laden channel flows," Phys. Fluids **32**, 103302 (2020).

L. F. Mortimer, D. O. Njobuenwu, and M. Fairweather, "Near-wall dynamics of inertial particles in dilute turbulent channel flows," Phys. Fluids **31**, 063302 (2019).

L. F. Mortimer, D. O. Njobuenwu, and M. Fairweather, "Agglomeration dynamics in liquid–solid particle-laden turbulent channel flows using an energy-based deterministic approach," Phys. Fluids **32**, 043301 (2020).

R. D. Moser, J. Kim, and N. N. Mansour, "Direct numerical simulation of turbulent channel flow up to $Re_\tau = 590$," Phys. Fluids **11**, 943–945 (1999).

B. Oesterle and A. Petitjean, "Simulation of particle-to-particle interactions in gas solid flows," Int. J. Multiphase Flow **19**, 199–211 (1993).

Y. Pan and S. Banerjee, "Numerical simulation of particle interactions with wall turbulence," Phys. Fluids **8**, 2733–2755 (1996).

J. J. Riley and G. S. Patterson, "Diffusion experiments with numerically integrated isotropic turbulence," Phys. Fluids **17**, 292–297 (1974).

L. Schiller and A. Naumann, "Fundamental calculations in gravitational processing," Z. Ver. Dtsch. Ing. **77**, 318–320 (1933).

M. Sommerfeld, "Validation of a stochastic Lagrangian modelling approach for inter-particle collisions in homogeneous isotropic turbulence," Int. J. Multiphase Flow **27**, 1829–1858 (2001).

K. D. Squires and J. K. Eaton, "Preferential concentration of particles by turbulence," Phys. Fluids A **3**, 1169–1178 (1991).

J. Tripathi, B. Vasu, R. Subba Reddy Gorla, A. J. Chamkha, P. V. S. N. Murthy, and O. Anwar Beg, "Blood flow mediated hybrid nanoparticles in human arterial system: Recent research, development and applications," J. Nanofluids **10**, 1–30 (2021).

M. Trojanowicz, K. Kołacińska, and J. W. Grate, "A review of flow analysis methods for determination of radionuclides in nuclear wastes and nuclear reactor coolants," Talanta **183**, 70–82 (2018).

B. Vreman, B. J. Geurts, N. G. Deen, J. A. M. Kuipers, and J. G. Kuerten, "Two-and four-way coupled Euler–Lagrangian large-eddy simulation of turbulent particle-laden channel flow," Flow, Turbul. Combust. **82**, 47–71 (2009).

P. Wang, J. Li, and X. Zheng, "The effect of gravity on turbulence modulation in particle-laden horizontal open channel flow," Phys. Fluids **33**, 083315 (2021).

Y. Yamamoto, M. Potthoff, T. Tanaka, T. Kajishima, and Y. Tsuji, "Large-eddy simulation of turbulent gas–particle flow in a vertical channel: Effect of considering inter-particle collisions," J. Fluid Mech. **442**, 303–334 (2001).

T. Zahtila, L. Chan, A. Ooi, and J. Philip, "Particle transport in a turbulent pipe flow: Direct numerical simulations, phenomenological modelling and physical mechanisms," J. Fluid Mech. **957**, A1 (2023).

F. Zhao, W. K. George, and B. G. van Wachem, "Four-way coupled simulations of small particles in turbulent channel flow: The effects of particle shape and Stokes number," Phys. Fluids **27**, 083301 (2015).

06 November 2023 12:05:03